Digitized Theses   Digitized Special Collections

1967

Vhf Studies Of The Lower Ionosphere

Frank Harry Palmer

Recommended Citation

VHF STUDIES OF THE LOWER IONOSPHERE

by

Frank Harry Palmer

Department of Physics

Submitted in partial fulfillment

of the requirements for the degree of

Doctor of Philosophy

Faculty of Graduate Studies

The University of Western Ontario

London, Canada.

June 1967

ABSTRACT

Radio auroral scattering is regularly observed on an Ottawa – London oblique scatter circuit operating at a frequency of 40.35 MHz. These events appear to have the same gross characteristics as type A_1 forward scattered signals. The spatial and temporal characteristics of several events have been examined by performing a correlation analysis of the amplitude records obtained from spaced antennas. Computed spatial correlation functions imply scale sizes ranging from near the wavelength used to over 100 metres. It is shown that these observations are governed by the dimensions of the scattering region as a whole, and not by the dimensions of the individual scatterers. It has been found that at least two types of event are observed. One type shows typical fading rates of 15 Hz., and an east to west drift of the amplitude pattern of between 400 and 1600 m/sec. The detailed characteristics of this type of event are consistent with the hypothesis of scattering by ion-acoustic wave instabilities. The other type of event exhibits a fading spectrum which extends to beyond 100 Hz., and shows a variety of amplitude pattern drift directions. Drift velocities range from 0.5 to 10 Km/sec. This type of event is not consistent with either scattering by ion-acoustic wave instabilities or by simple inhomogeneities in electron density which drift with the local wind velocity.

iii

ACKNOWLEDGEMENTS

TABLE OF CONTENTS

LIST OF ILLUSTRATIONS

REFERENCES

Awe, O., (1964), J.A.T.P., 26, 1239.

Blevis, B.C. and Collins, C., (1965), Radio Aurora. In "Physics of
the Earth's Upper Atmosphere". Hines, C.O., Ed., Prentice Hall, Inc.

Booker, H.G., (1960), Radar Studies of the Aurora. In "Physics of
the Upper Atmosphere". Ratcliffe, J.A., Ed., Academic Press,
New York.

Booker, H.G., et al., (1955), J. Geophys. Res., 60, 1.

Born, M., and Wolf, E., (1959), Principles of Optics, Pergamon Press,
New York.

Bowles, K.L., et al., (1963), J. Geophys. Res., 68, 2485.

Briggs, B.H., et al., (1950), Proc. Phys. Soc., 63, 106.

Collins, C., and Forsyth, P.A., (1959), J.A.T.P., 13, 315.

Davis, T.N., and Hicks, G.T., (1964), J. Geophys. Res., 69, 1931.

Egeland, A., (1963), Ark. för Geophys., 4, 171.

Farley, D.T., (1963), J. Geophys. Res., 68, 6083.

Gadsden, M., (1967), Planet. Space Sci., 15, 689.

Hultqvist, B., and Egeland, A., (1964), Space Sci. Rev., 3, 27.

Leadabrand, R.L., (1965), N.B.S. J. of Res., 69D, 959.

Lyon, G.F., (1967), Private communication.

Lyon, G.F., and Forsyth, P.A., (1962), Can. J. Phys., 40, 749.

Mitra, S.N., (1949), Proc. I.E.E., part III, 96, 441.

Moorcroft, D.R., (1966), Planet. Space Sci., 14, 269.

Paulson, K.V., and Shepherd, G.G., (1966), Can. J. Phys., 44, 921.

Phillips, G.J., and Spencer, M., (1955), Proc. Phys. Soc., 68, 481.

Ratcliffe, J.A., (1956), Repts. Prog. Phys. XIX, 188.

Ratcliffe, J.A., and Weekes, K., (1960), The Ionosphere. In "Physics of the Upper Atmosphere". Ratcliffe, J.A., Ed., Academic Press, New York.

Rice, S.O., (1944), Bell Syst. Techn. J., 23, 282; 24, 46.

CHAPTER I

INTRODUCTION

1.1 Historical

Visual aurora have been observed for many thousands of years; descriptions being given before Roman times. Scientific observations are of a comparatively recent origin, and were originally of an entirely optical nature. Since World War Two however, significant advances in our knowledge of the auroral ionosphere have been made with the use of radio techniques.

A great deal of work has been done in the past ten years in correlating auroral events, observed on both forward and backscatter systems, with other geomagnetic and solar activity (see, for example, review articles by Ratcliffe, 1960; Hultqvist and Egeland, 1964; Blevis and Collins, 1965). Much of the data used has been scaled from low time resolution paper and film records. As a result, only the gross characteristics of any event could be recognized and evaluated. Nonetheless, a certain amount of information has been gained about the nature of the scattering processes responsible for the occurrence of these events from such studies as the angular and frequency dependences of the received signal amplitudes. It has become apparent (see, for example, the review paper by Egeland, 1963) that weak

1

scattering is capable of explaining most of the observations, and that critical reflection, if it occurs at all, is operative for only limited periods of time at the lower end of the VHF band. The detailed nature of the weak scattering is still subject to considerable uncertainty. Forward scatter and radar studies indicate that more than one type of echo can be received (Collins and Forsyth, 1959), and this raises the possibility that more than one type of scattering mechanism may exist.

1.2 Scattering Mechanisms

Two fundamentally different types of weak scatterers have been postulated. One type consists of a random array of field-aligned irregularities in electron density while the other type consists of a family of plane waves in electron density arising as a result of ion-acoustic wave instabilities in the auroral electrojet. Both types of scatterers will give rise to aspect sensitive echoes such as those usually observed. The ion-acoustic wave theory (Farley, 1963) is of recent origin and its full implications with respect to auroral observations have not yet been fully explored. This theory has had much success in the interpretation of VHF scatter echoes from the equatorial electrojet, and some evidence has been presented (Leadabrand, 1965; Gadsden, 1967) that such waves contribute to the production of auroral echoes. It has also been shown (Moorcroft, 1966) that multiple frequency observations of radio aurora (Lyon and Forsyth, 1962) are not easily explicable in terms of a random array of scatterers and that a wave-generating process appears to provide

the most reasonable explanation of the observations of radio auroral frequency dependence. On the other hand, amplitude measurements as a function of scattering angle (Lyon, 1967) are consistent, at some times, with scattering by field-aligned irregularities while at other times they are consistent with scattering by wave-like structures. This observation again raises the possibility that different scattering mechanisms may be operative at different times.

1.3 Present Work

This thesis represents an attempt to shed further light on the nature of the scattering processes responsible for the production of the auroral scatter events observed on VHF scatter circuits.

Information concerning the fine structure of auroral ionization may be obtained from a study of the detailed nature of the scattered field on the ground at the receiving site. This type of study has been carried out for some time in work on F region irregularities (Mitra, 1949). In these cases, radio stars, satellites, and ground based vertical incidence sounders were used as sources of radiation and the distribution of received signal amplitude was investigated with an array of spaced antennas on the ground. From such measurements it is possible to deduce the scale size of the structure of the scattered field on the ground, the velocity of the pattern over the ground, and the rate at which the pattern is changing with time. These parameters may be related to the structure of the scattering regions themselves.

Little work of this type has been done on aurorally propagated

signals since the initial study by Collins and Forsyth (1959).

In the present study, measurements were made upon oblique scatter events resulting from disturbances in the auroral ionosphere. Specifically, the spatial and temporal variations of the received signal amplitude were studied, using records obtained from spaced antennas on the Ottawa – London oblique scatter circuit. Characteristics of both the individual scatterers and of the scattering regions as a whole were then inferred from the observations.

Chapter Two contains a review of the techniques used in the signal analysis, and a discussion of the relationship between the detected signals which are actually analyzed and the original distribution of RF amplitude at the receiving site. Chapter Three describes the equipment used and gives details of the analysis. This is followed by a discussion of the possible experimental errors and the reliability of the results. The raw experimental data is described in Chapter Four, while Chapter Five is devoted to a discussion of the characteristics of the scattered fields as determined from this data. The effect of a finite scattering region upon the nature of the resultant scattered field is discussed in Chapter Six. This is followed by a discussion of the characteristics of the scattered fields in terms of possible scattering mechanisms and scattering regions as a whole. A summary of the findings, and conclusions drawn from the present work, are presented in the final chapter.

1.4 Definitions

Any radio-auroral investigations require, basically, a transmitter and a receiver. A transmitter with its associated receiver at

the same location are referred to as a <u>radar</u>, or <u>monostatic</u> system.
If the transmitter and receiver are not at the same location they
are referred to as a <u>bistatic</u> or <u>oblique</u> scatter system. A <u>forward
scatter</u> system is one in which the scattering angle is close to 180
degrees while one in which the scattering angle is closer to zero is
referred to as a <u>backscatter</u> system of which a radar is a special case.

If scattering occurs at a sufficiently high altitude, diffusion
of the charged particles is controlled predominantly by the earth's
magnetic field and not by collisions as at lower altitudes. The
magnetic field constrains horizontal diffusion, but leaves the
particles free to move along the field lines. The result is field-
aligned structure in which the inhomogeneities in electron density
have much larger dimensions in the direction of the magnetic field
than at right angles to it. The <u>aspect angle</u> is defined as the
angle between the field lines at the point of reflection and the line
bisecting the angle formed by the transmitter, reflection point, and
receiver. Reflection or scattering tend to occur when the aspect
angle is close to 90 degrees. This phenomenon is called <u>aspect
sensitivity</u>. Similar effects are observed in scattering from wave-
like plasma instabilities whose direction of propagation is
controlled by the magnetic field and by the electrojet current
direction.

CHAPTER II

THEORETICAL CONSIDERATIONS

The entire record analysis is carried out using correlation techniques. With the use of these techniques, quantitative descriptions may be provided for the statistical properties of the signals analyzed.

2.1 Correlation Functions

Consider two functions $f(t)$ and $g(t)$. In the present context these usually represent received amplitude as a function of time. A measure of the strength of the relationship between $f(t)$ and $g(t)$ is given by the covariance of $f(t)$ and $g(t)$. This may be written as

$$\sigma(f,g) = \overline{f(t).g(t)} \qquad 2.1$$

This is usually normalized so as to have a maximum value of unity if $f(t)$ and $g(t)$ are identical. The resulting crosscorrelation coefficient is thus defined as

$$\rho(o) = \overline{f(t).g(t)} \Big/ \left[\overline{f^2(t)} \cdot \overline{g^2(t)} \right]^{\frac{1}{2}} \qquad 2.2$$

If $f(t)$ and $g(t)$ are unrelated, $\rho(o) = 0$. It is useful to extend this definition to include cases in which the two signals being compared are subject to increasing relative time displacements. The cross-correlation function is defined as

$$\rho(\tau) = \overline{f(t)g(t+\tau)^*} \Big/ \left[\overline{f(t)^2} \cdot \overline{g(t)^2} \right]^{\frac{1}{2}} \qquad 2.3$$

6

where τ is the _lag_, or relative time displacement, between $f(t)$ and $g(t)$. This function exhibits a maximum at lag τ^* if $f(t)$ and $g(t)$ are similar, but displaced in time by an amount τ^*. If $f(t) \equiv g(t)$, ρ is termed the _autocorrelation function_ of $f(t)$.

If $f(t)$ is a slowly varying function, τ must vary over a large range in order to produce an appreciable change in the value of ρ. Conversely, if $f(t)$ varies rapidly with time, large changes in ρ occur as a result of small changes in τ. This is consistent with the fact that the autocorrelation function may be shown to be the Fourier transform of the power spectrum $\left|F(\omega)\right|^2$ of $f(t)$. An important special case is where a function has an autocorrelation function which may represented by

$$\rho(\tau) = \exp - (\tau^2/a^2) \qquad\qquad 2.4$$

The width (1/e point) of this function is at $\tau^* = a$.

The corresponding power spectrum of the function is represented by

$$\left|F(\omega)\right|^2 = \exp - (\pi^2\omega^2 a^2) \qquad\qquad 2.5$$

which has a width

$$\omega = 1/\pi a = 1/\pi\tau^* \qquad\qquad 2.6$$

The spectrum width may thus be found from either the spectrum itself or from the autocorrelation function. The corresponding transform of the crosscorrelation function is known as the _cross-spectrum_ of $f(t)$ and $g(t)$.

A correlation function may be looked upon as a plot of correlation coefficients as a function of lag. In the present context, if a series of correlation coefficients are computed between the signals received at different antenna separations L, the results may be plotted as a

function of L to produce the spatial autocorrelation function of the signal distribution along the line of the antennas. The zero-lag crosscorrelation coefficients must be used in these calculations since they represent the distribution of received signal amplitude, independent of change with time or drift of the amplitude pattern. Implicit in this type of measurement is the assumption of the ergodic hypothesis. In the present situation, this implies that the statistics of a signal received as a function of time at a single point in space are assumed to be the same as the statistics of the signal distribution in space at a fixed point in time.

The scale size of a randomly varying signal distribution on the ground may be defined as the distance L* at which the spatial auto-correlation function falls to 1/e. L* gives a measure of the smallest structure which contributes appreciably to the observed amplitude distribution. If the structure on the ground is spatially periodic, the spatial autocorrelation function is also periodic, with the same period.

Motion of the scattering region as a whole causes a drift of the amplitude pattern over the ground. Since the transmitter and receiver of a scatter circuit are usually equidistant from the scattering region, the velocity of the diffraction pattern over the ground is approximately twice that of the scattering region itself. A component of the velocity of the diffraction pattern, along the line joining two antennas, may be found from a measurement of the lag T at which the crosscorrelation function of the two signals has a maximum.

2.2 On the Nature of Detected Signals

Care must be taken if the characteristics of the RF field on the

ground are to be correctly inferred from an analysis of the fading records. This point arises because it is not the RF field itself which is studied, but the output from an approximately square law detector.

Let the RF signal at the antenna be represented by $g(t)$. This signal has a power spectrum $w(f)$. It can be shown (Rice, 1944) that the power spectrum, $W(f)$, of the detected signal is of the form

$$W(f) = \alpha^2 \int_{-\infty}^{+\infty} w(x)w(f-x)\ dx \qquad 2.7$$

where α is a constant.

If it is assumed that the spectrum $w(f)$ has a gaussian envelope, i.e.

$$w(f) = c_1 \exp - f^2/a^2 \qquad 2.8$$

then the spectrum of the detected signals, which is actually measured, is of the form

$$W(f) = c_2 \exp - f^2/2a^2 \qquad 2.9$$

that is, the measured power spectrum has an envelope which is approximately the square root of the envelope of the power spectrum of the original RF signal. It follows that the measured widths of the fading spectra are approximately $\sqrt{2}$ times the widths of the fading spectra of the original RF field. Similarly, the measured correlation functions are approximately the squares of the correlation functions describing the original RF signals, and are thus $1/\sqrt{2}$ times the widths of the functions describing the RF field. Since time displacements of the peaks in the computed crosscorrelation functions are not changed by the detection process, apparent velocity measurements remain unchanged.

If the RF signals have periodic components, it is easily shown that the computed wavelengths of the auto- and crosscorrelation functions of these signals are the same as those describing the RF signal itself.

CHAPTER III

EQUIPMENT AND RECORD ANALYSIS

For the type of analysis described in this thesis a high-resolution record of received signal amplitude as a function of time is required at two or more points on the earth's surface. The circuit used was the Ottawa - London oblique scatter circuit. The transmitted frequency was 40.35 MHz and the radiated power was 100 watts.

Three events were selected for analysis. They will be referred to as events A, B, and C in order of occurrence. The transmitting and receiving antennas used for event A were identical five-element yagis with half-power beamwidths of approximately forty-five degrees. For events B and C, the transmitting antenna consisted of an array of five-element yagis with a resultant beamwidth of approximately twelve degrees. Receiving antennas were again single five-element yagis. The detailed geometry of these circuits is shown in Fig. 3.1. All antennas were placed at such a height above ground that the main lobes intersected at a height of 100 km in the centre of the region of interest. The volume of sky, at 100 km, illuminated by both the transmitting and receiving antennas is indicated by the hatched region of the diagram. Superimposed upon this are contours of constant aspect angle.
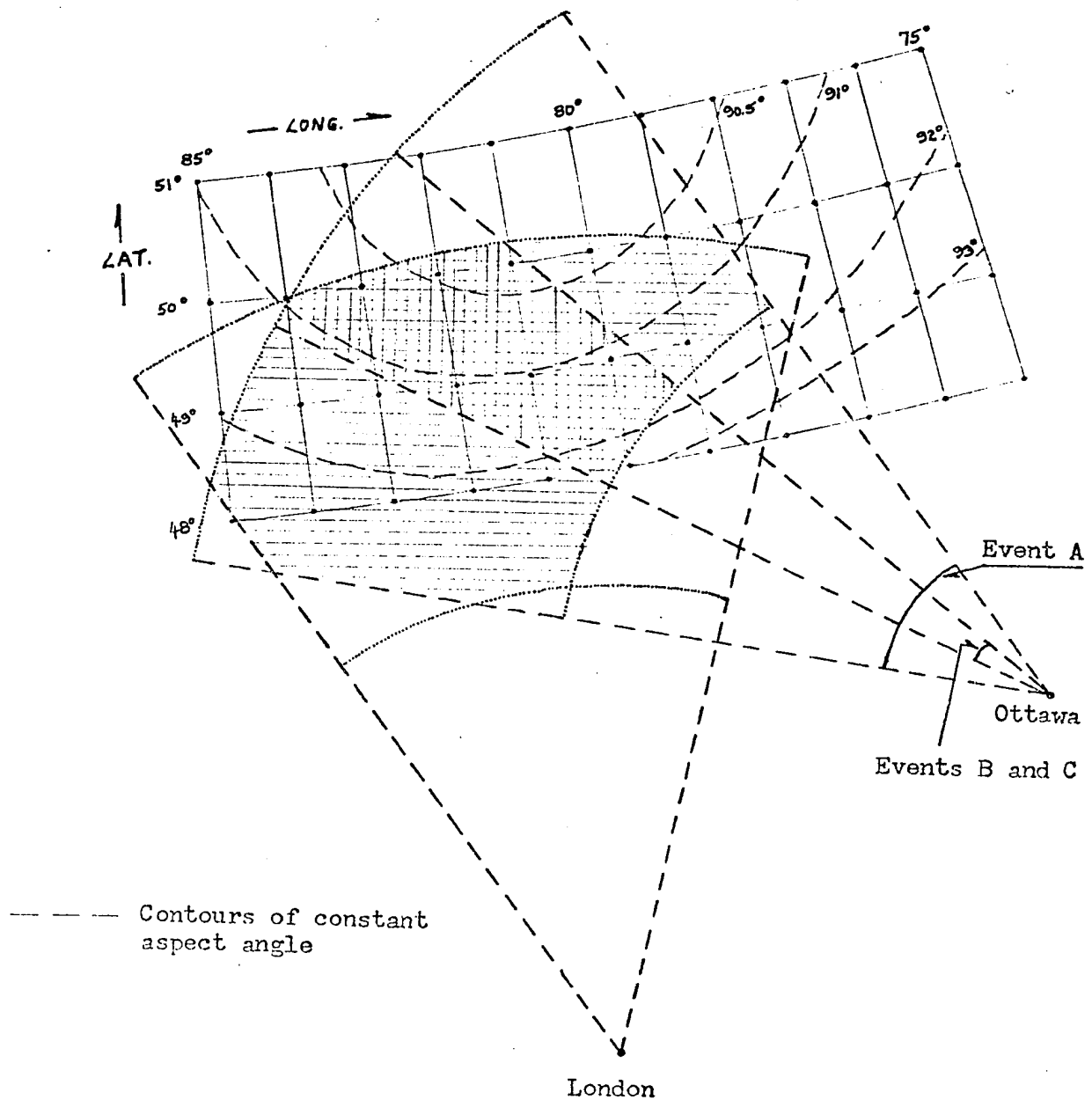
Figure 3.1

Geometry of the Ottawa and London Antenna Systems

The details of the recording and analysis of event A also differed from those of the other two events and so will be described separately.

3.1   Event A

Two antennas were placed two wavelengths (15 metres) apart transverse to the expected direction of arrival of the scattered signals. Each antenna was fed to a separate Ferranti – Packard model 155 VHF receiver with a bandwidth of 1.2 KHz. The receiver sensitivities were cosmic noise limited at the frequency used. The intermediate frequency outputs of the two receivers were then detected and recorded on magnetic tape after AM – FM conversion. This conversion was necessary because of the poor amplitude fidelity of the tape recorders available at the time this event was recorded. The fidelity of information recorded in the FM mode is limited by the tape speed stability. The specified wow and flutter for these machines was less than 0.7%. This was verified by comparison of the amplitudes of reproduced test signals with those of the original signals before recording. For purposes of analysis, the recorded signals were converted back to their original form by FM – AM conversion and then recorded on a Sanborn two channel chart recorder using a chart speed of 100 mm per second.

Fifty-two segments of signal, each of $2\frac{1}{2}$ seconds duration, were thus reproduced every forty seconds throughout the duration of the event. The minimum useable rms signal amplitude was taken as approximately 0.15 microvolts in order to maintain a signal to noise ratio of at least 15 db on the final record.

Inspection of the final record showed that negligible power was contained in frequencies above 50 Hz, so it was decided to scale the record at intervals of 10 milliseconds, resulting in a total of 250 data points per channel per segment of signal. For each set of signal pairs, the autocorrelation function of each signal, the power spectrum of each signal, and the cross correlation function of the pair were computed using the IBM 7040 computer of the University Computing Centre. The program used was a modified version of program BMD02T, originally written by the Department of Biomedical Sciences of the University College of Los Angeles.

The frequency response of the entire system was determined by the frequency response of the AM — FM, FM — AM converters. The power frequency response is plotted in Figure 3.2. The computed spectrum and correlation function widths were then corrected, where necessary, using the results of this plot.

3.2 Events B and C

In these two cases, three antennas were placed transverse to the expected direction of arrival of the scatter signals. They were spaced in such a way as to provide spacings of 2, 4, and 6 wavelengths. Three Hammarlund SP-600 receivers were used, which as for the Ferranti-Packard receivers, were cosmic noise limited at 40.35 MHz. The bandwidths used were 1.3 KHz. The intermediate frequency outputs of the receivers were detected and the resulting fluctuating DC voltages were recorded, in the FM mode, on a four channel Precision Instruments model 6100 instrumentation tape recorder. A voice time count was recorded on the fourth channel.

Figure 3.2

Power Frequency Response of
Equipment used in Recording

Event A
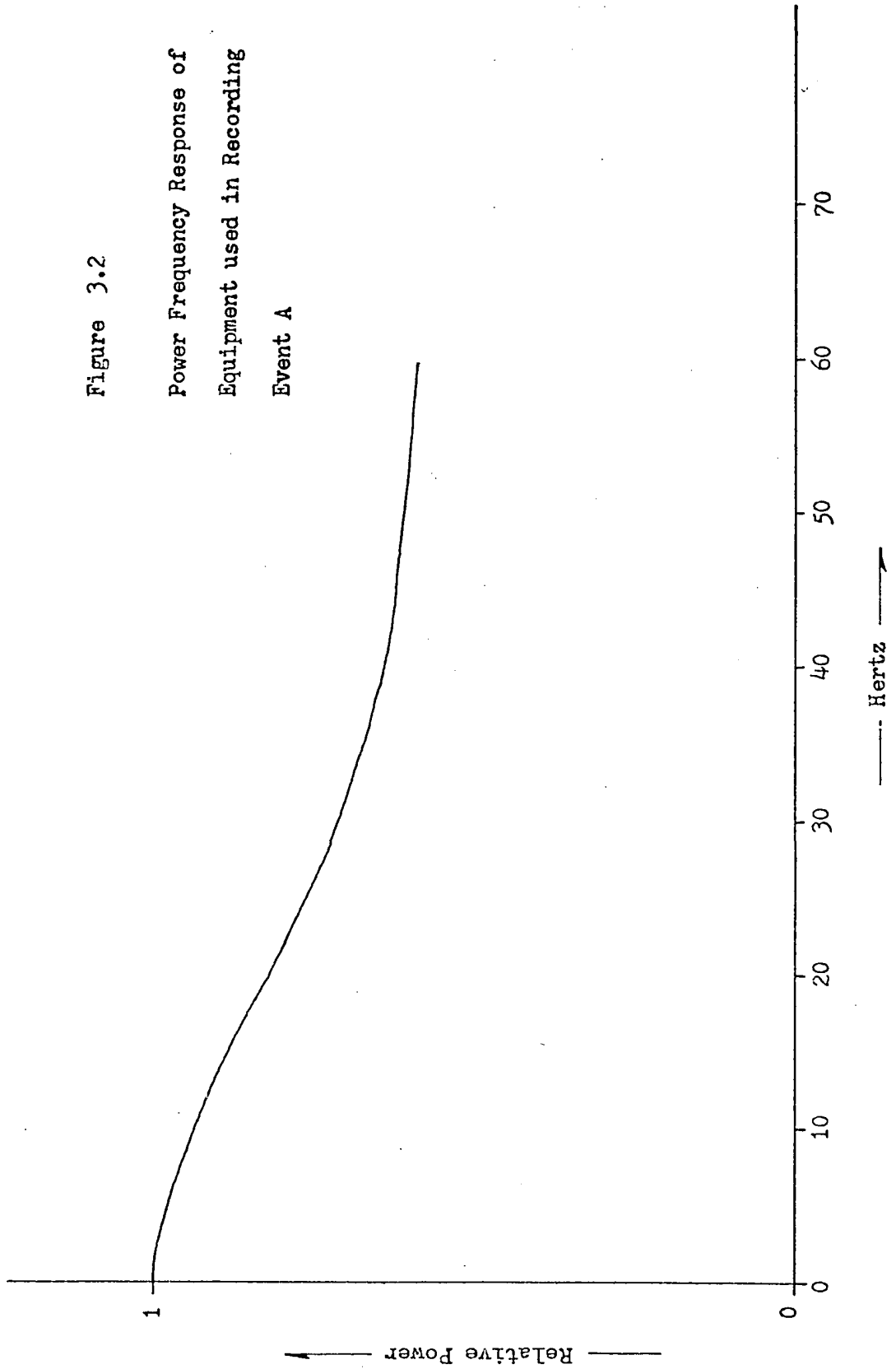
The entire record analysis in these two cases was carried out using a Noratom 'ISAC' analogue statistical analyzer. For analysis, the three recorded signals were simultaneously transcribed from the tape recorder to a closed tape loop within the analyzer. For each event three autocorrelation functions, three crosscorrelation functions between different pairs of antennas, and sample power spectra were computed. All results were plotted automatically on an X-Y plotter. The frequency response of the analyzer is flat from DC to 200 Hz. The overall frequency response of the system is determined by the frequency response of the detector used at the receiver output. The frequency response of the entire system is shown in Fig. 3.3. From this, corrections were applied to the final computations.

For the highest accuracy in computation it is desirable to 'fill' as much of the frequency range of the statistical analyzer as possible. Event C had frequency components extending to over 100 Hz so that segments of the three signal channels were transcribed onto the closed tape loop with a 1:1 tape speed ratio. Segments of signal analyzed were five seconds in length. Forty-eight such segments were analyzed throughout the event.

Event B had a much narrower bandwidth, with little power above 25 Hz. Segments of this signal were therefore transcribed onto tape loops within ISAC moving at 1/8 normal speed. Forty seconds of data could be recorded on a five second loop in this manner. All frequency components were translated upward by a factor of eight when the tape was played back at full speed for analysis. This essentially filled the available bandwidth of the analyzer. Twenty-five such forty

Figure 3.3

Power Frequency Response of

Equipment used in Recording

Events B and C
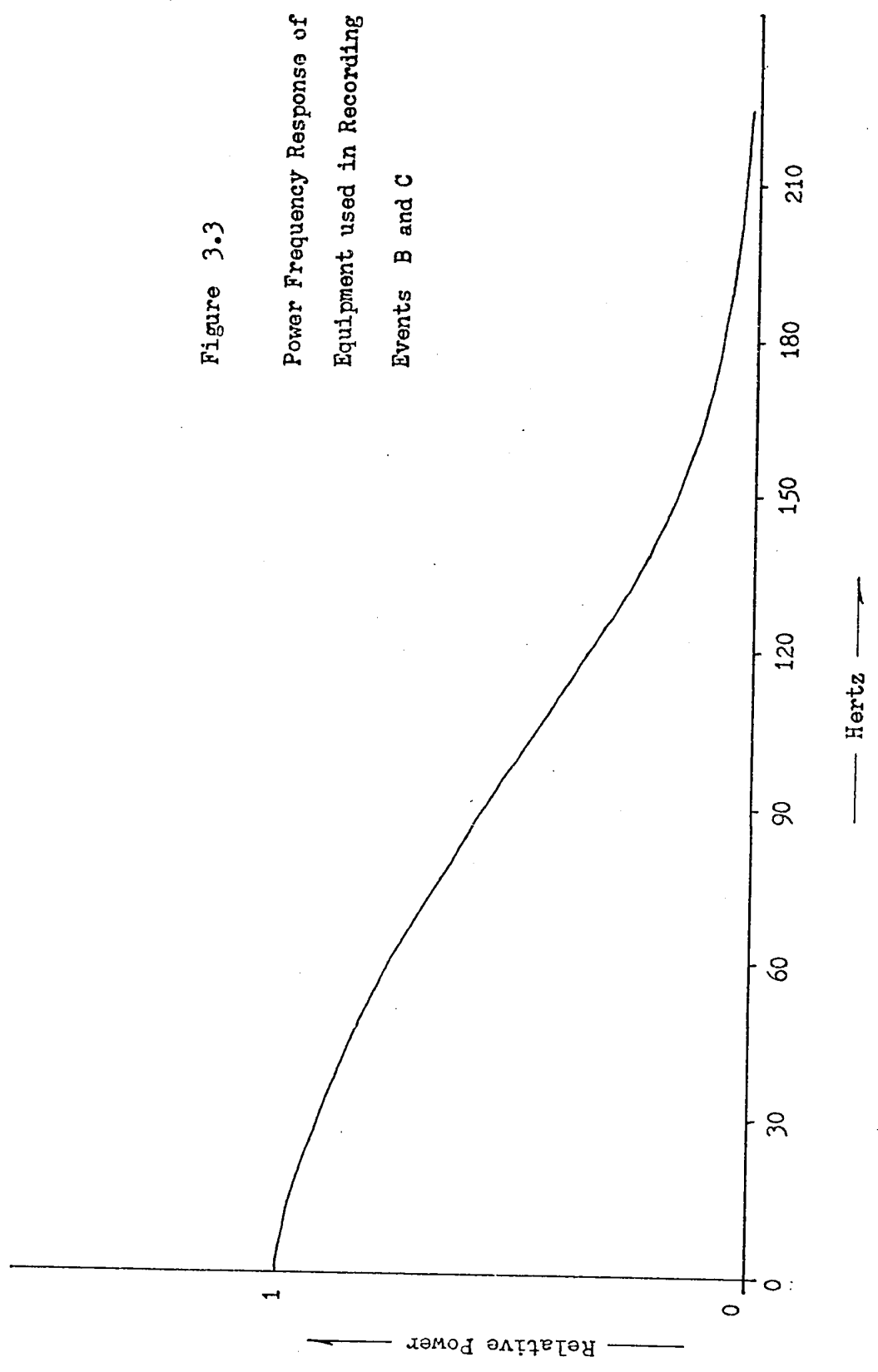
second samples were recorded throughout the event. As was the case

for event A, only rms signal amplitudes above approximately 0.15

microvolts were used for analysis in order to maintain an adequate

signal to noise ratio.

Disregarding, for the moment, statistical errors dependent upon

sample length and spectrum width, the computational accuracy of the

ISAC analyzer is stated by the manufacturer to be less than 1%. The

reproducibility of the computations was checked to be within 1%.

The time resolution of the ISAC analyzer is 0.8 msec at full speed.

The reproducibility of crosscorrelation function time displacements

was checked to be approximately equal to the time resolution of the

device.

3.3 Statistical Errors in the Computations

For all signals recorded it is assumed that there exist 'true'

auto- and crosscorrelation functions. Any practical computation

however, yields only approximations to these ideal functions. The

degree to which the computed functions agree with the ideal functions

depends upon the sample length used, the frequency bandwidth of the

signal, and the number of sample points used per unit of time. It is

the intent of this discussion to estimate how closely the computations

carried out in this experiment approximate the ideal functions, and to

estimate the significance of any features shown by these functions.

The standard error, σ_r, of the calculated correlation r, is

usually estimated from the expression

$$\sigma_r = (1 - r^2) \Big/ (N - 1)^{\frac{1}{2}} \qquad\qquad 3.1$$

This expression has been criticized by Awe (1964), who points out that r is usually taken to represent the computed correlation coefficient whereas it should in fact represent the true correlation coefficient which is not known a priori. The difference between the computed value of r and the true value of r may become large as N becomes small. From the description of the present work which follows, it would appear that the above expression is of sufficient accuracy for the values of N used in the present work.

To determine the rms deviation of points on a computed cross-correlation function as a function of sample length random noise was recorded in three different ways.

a. Five seconds of signal were recorded directly onto a five second tape loop running at normal speed.

b. Fifteen seconds of signal were recorded directly onto a fifteen second tape loop running at normal speed.

c. Forty seconds of signal were recorded onto a five second tape loop running at 1/8 normal speed.

The power spectrum of cosmic noise has been measured. With the receiving system used for these tests cosmic noise power is down 3 db at 90 Hz. Taking this frequency as a measure of the bandwidth of the signal it is possible to calculate the effective number of sample points in each of the above cases. Counting two sample points per cycle for the highest frequency component of the signal, the effective number of sample points in case (a) is 900, and in case (b) 2700. In case (c) the spectrum width of the replayed signal is theoretically 540 Hz, but this is limited to 200 Hz by the input lowpass filter

of the ISAC. The effective number of sample points in this case
is thus 2000.

For each of the three cases two simultaneous channels were cross-correlated. Since $r \sim 0$, and N is large,

$$\sigma_r \sim \frac{1}{\sqrt{N}} \qquad\qquad 3.2$$

by Eqn. 3.1. The actual rms deviations were calculated in each case
from the computed functions. The results are shown in Table 3.1.

Trial	Number of Sample Points N	σ_r	
		Theory	Measured
a	900	.033	.053
b	2700	.019	.018
c	2000	.022	.021

Table 3.1

These results are considered to be in sufficient agreement to justify
the use of Eqn. 3.1 in computing the possible errors of the functions
considered here.

The number of sample points used in computing all the functions
in event A was 250. The corresponding rms deviation expected is thus
6.3%. The fading spectrum width of event B was approximately 15 Hz.
The signal was replayed at 8 times recorded speed for analysis,
resulting in an effective bandwidth of 120 Hz. The length of the
replayed signal sample was 5 seconds. The expected rms deviations
of the correlation functions is thus calculated to be approximately
2.9%. The fading spectrum width of event C was typically 75 Hz,
giving a possible rms deviation of 3.5%.

The effect of finite sample length upon the peaks observed in the auto- and crosscorrelation functions was next investigated. Samples of signal from event B were used, and the same crosscorrelation was computed for different sample lengths of signal.

a. A 15 second sample was recorded directly onto a long tape loop, and

b. A 40 second sample was recorded onto a tape loop at 1/8 normal speed.

The peak to peak amplitude of two different peaks in the cross-correlation function were computed for each of the two cases. The results are shown in the following table.

	P-P amplitude 15 sec loop	P-P amplitude 40 sec loop
1st Peak	0.35	0.33
2nd Peak	0.17	0.14

Table 3.2

If these peaks were due to a statistical fluctuation as a result of restricted sample length, the amplitudes of the peaks might be expected to decrease as the inverse square root of the sample length. The peaks in case (b) should then be $(15/40)^{\frac{1}{2}} = 0.61$ times the amplitude of the peaks in case (a). The observed ratios are:

a. 0.95

b. 0.83

The absolute differences of the amplitudes in both cases are of the same order as the expected rms deviations computed earlier. There is thus sufficient justification for regarding observed peaks as real and for having confidence in the computed amplitudes of the peaks.

CHAPTER IV

RESULTS

This chapter is devoted to a discussion of the raw data obtained. Each of the three events will be taken in turn.

4.1 Event A

This event occurred on the Ottawa - London circuit between 0130 and 0330 UT, April 9, 1965. The visual appearance of this event, as recorded on an Esterline - Angus recording milliammeter, is shown in Fig. 4.1.

As described in Chapter Three, fifty-two sample pairs of signal were analyzed throughout the event, using the IBM 7040 computer of the University Computing Centre. As well as the auto- and cross-correlation functions of the two signals, the mean amplitude of the signal received at each antenna in each $2\frac{1}{2}$ second interval was found. The zero-lag crosscorrelation coefficients as a function of time are shown in Fig. 4.2, and the amplitude, plotted on a linear scale, is shown as a function of time in Fig. 4.3.

The time resolution of the crosscorrelation functions was 10 milliseconds. With this limitation, no time displacements were observed on any crosscorrelation functions. Closer examination of
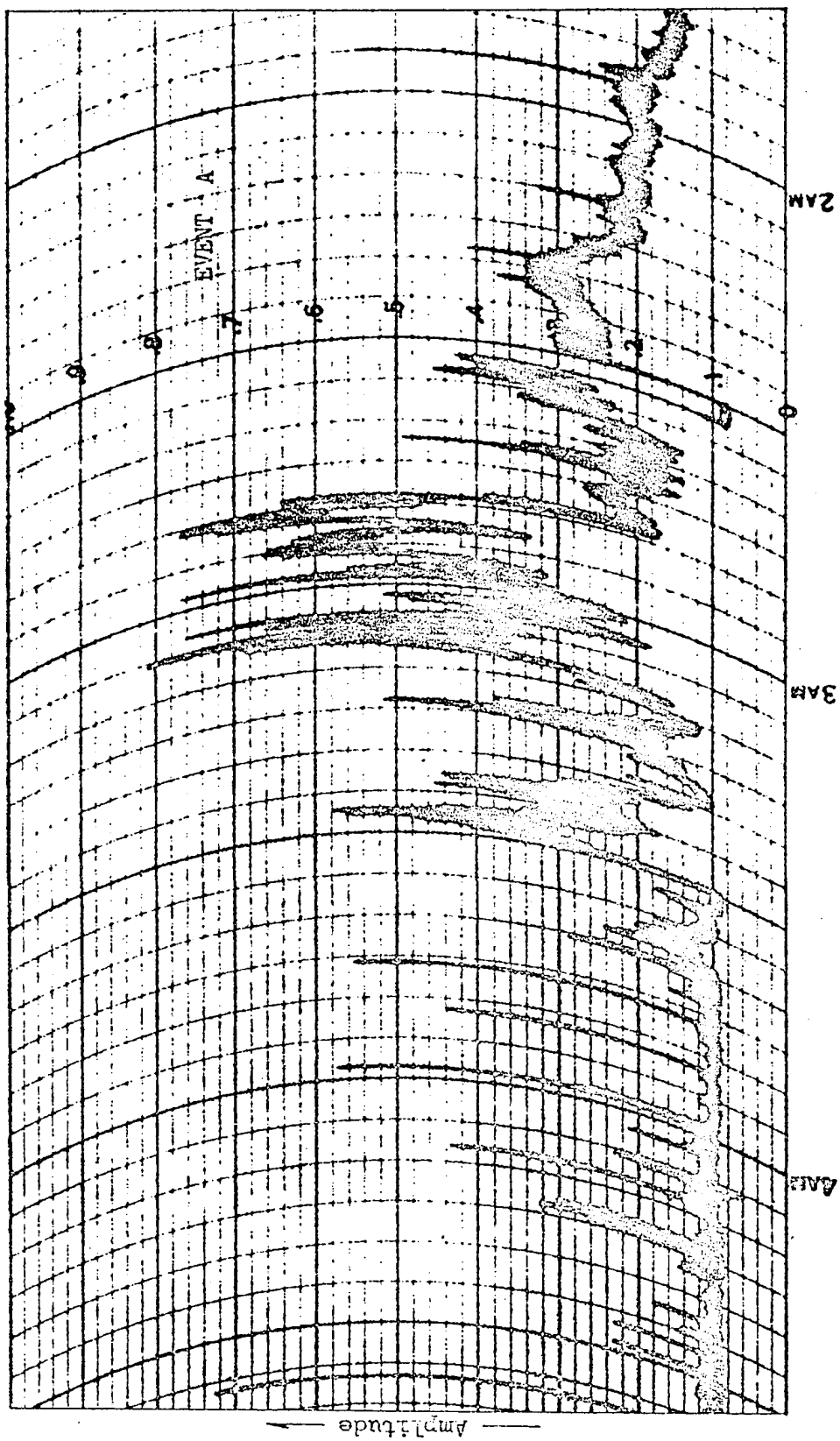
Figure 4.1.

Figure 4.2. Zero-lag Crosscorrelation Coefficients as a Function of Time

EVENT A

— Time in seconds —⟶

⟵ Zero Lag Crosscorrelation —
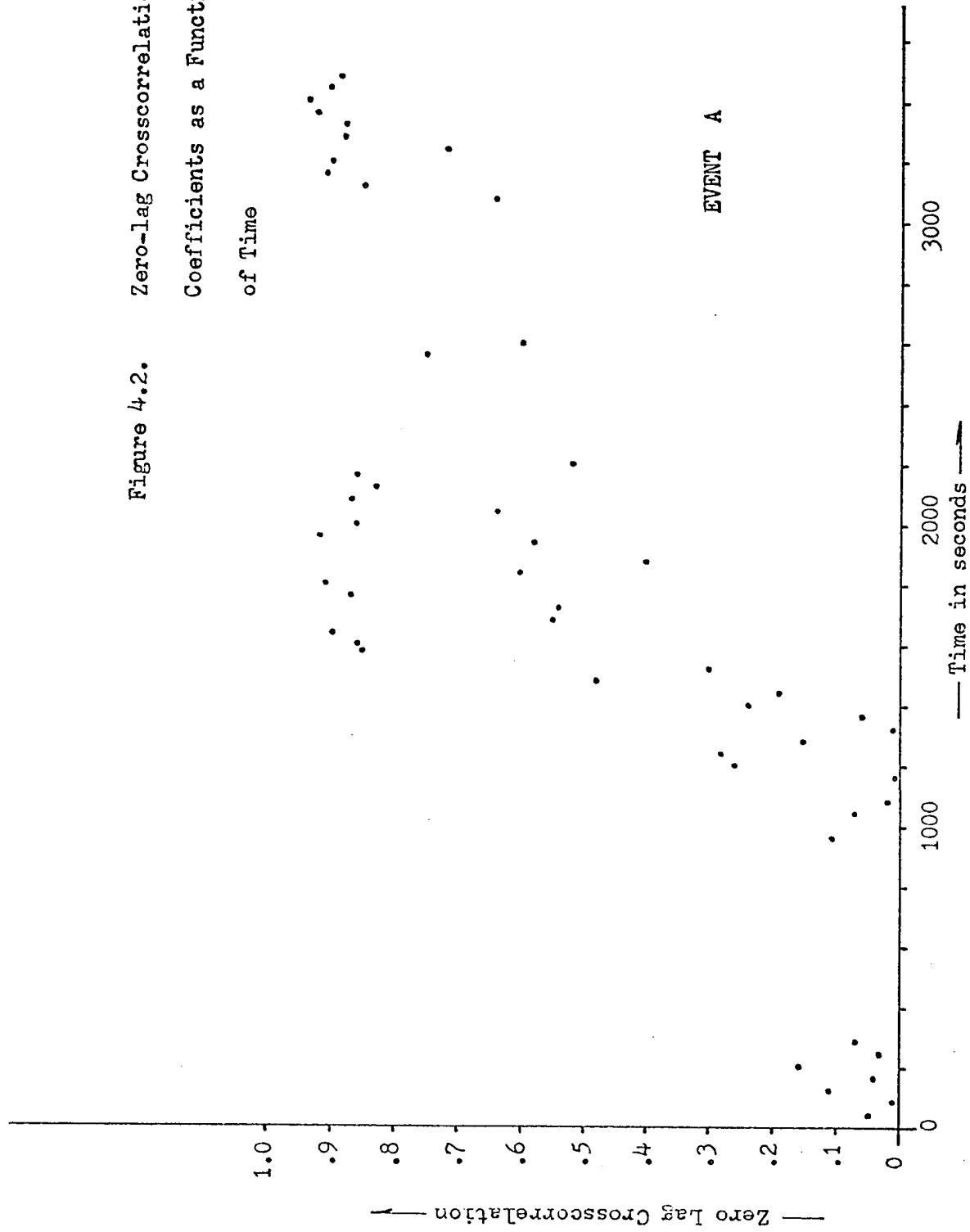
Figure 4.3   Amplitude of Event A

as a Function of Time
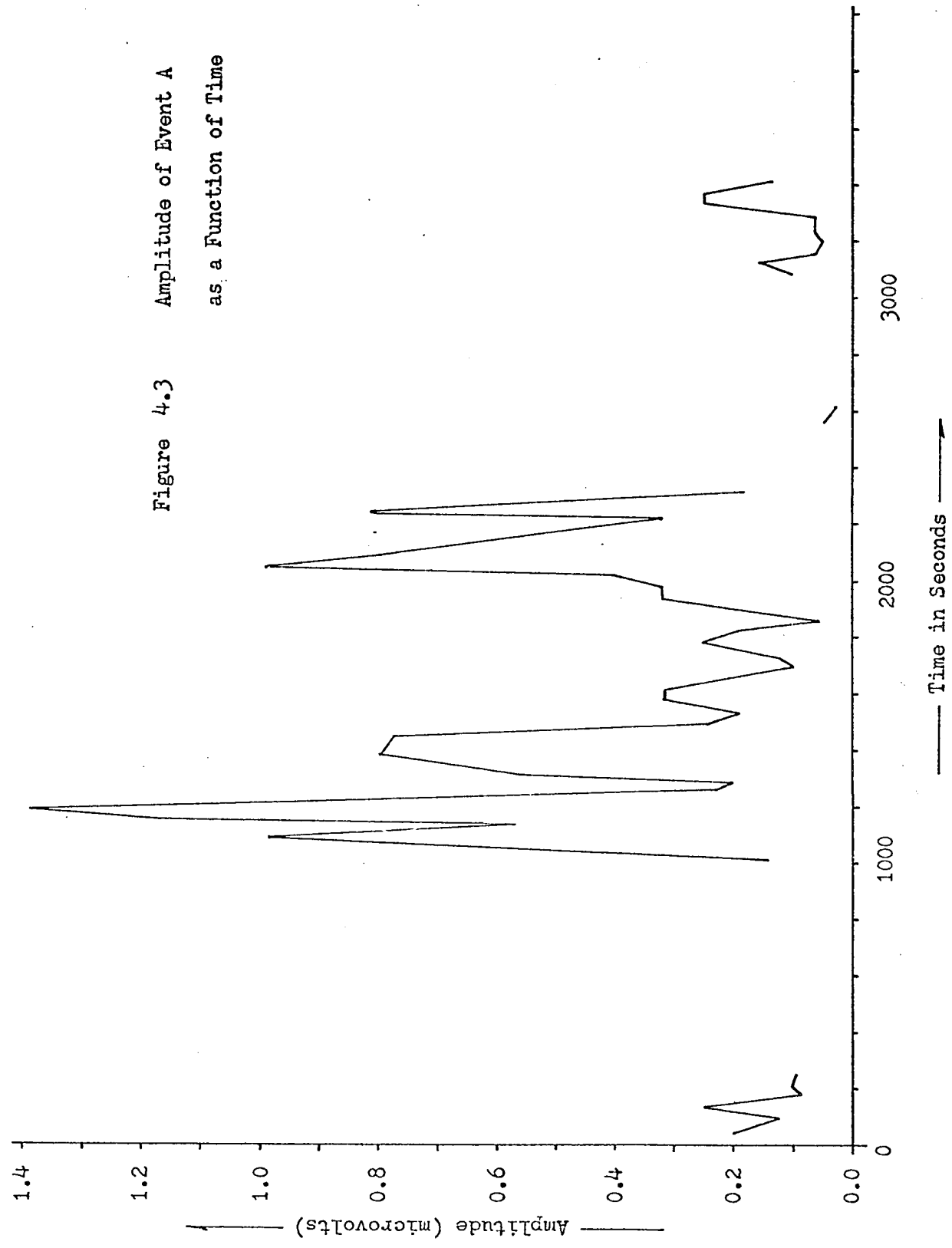
the amplitude – time records, during instances when the two signals were highly correlated, revealed that if time displacements existed between the two received signals, they were less than 2.5 msec during these periods.

It may be seen from Fig. 4.2 that the zero-lag crosscorrelation coefficients increase slowly during the course of the event. The transition from low to high correlation is not nearly as rapid as a visual examination of the records would indicate. This points out the care that must be exercised in appraising records without resorting to a thorough statistical analysis.

Because of the irregular nature of the envelopes of most of the spectra, the point at which the power first falls to 1/e of its maximum value does not necessarily give an accurate estimate of the width of the spectrum. For a gaussian spectrum, 84% of the power is contained in frequencies below the point at which the spectrum falls to 1/e. In practice then, the total power contained in a given spectrum was computed, as was the frequency below which was contained 84% of the power. This frequency was used as an estimate of the fading spectrum width. The resulting spectrum widths were then corrected for the finite bandwidth of the detector and finally multiplied by $1/\sqrt{2}$ in order to approximate the fading bandwidth of the original RF signal. The results are shown, plotted as a function of time, in Fig. 4.4.

4.2 Event B

This event took place on the Ottawa – London circuit between

Figure 4.4.

Fading Rates of RF Signals
at Antenna as a Function
of Time
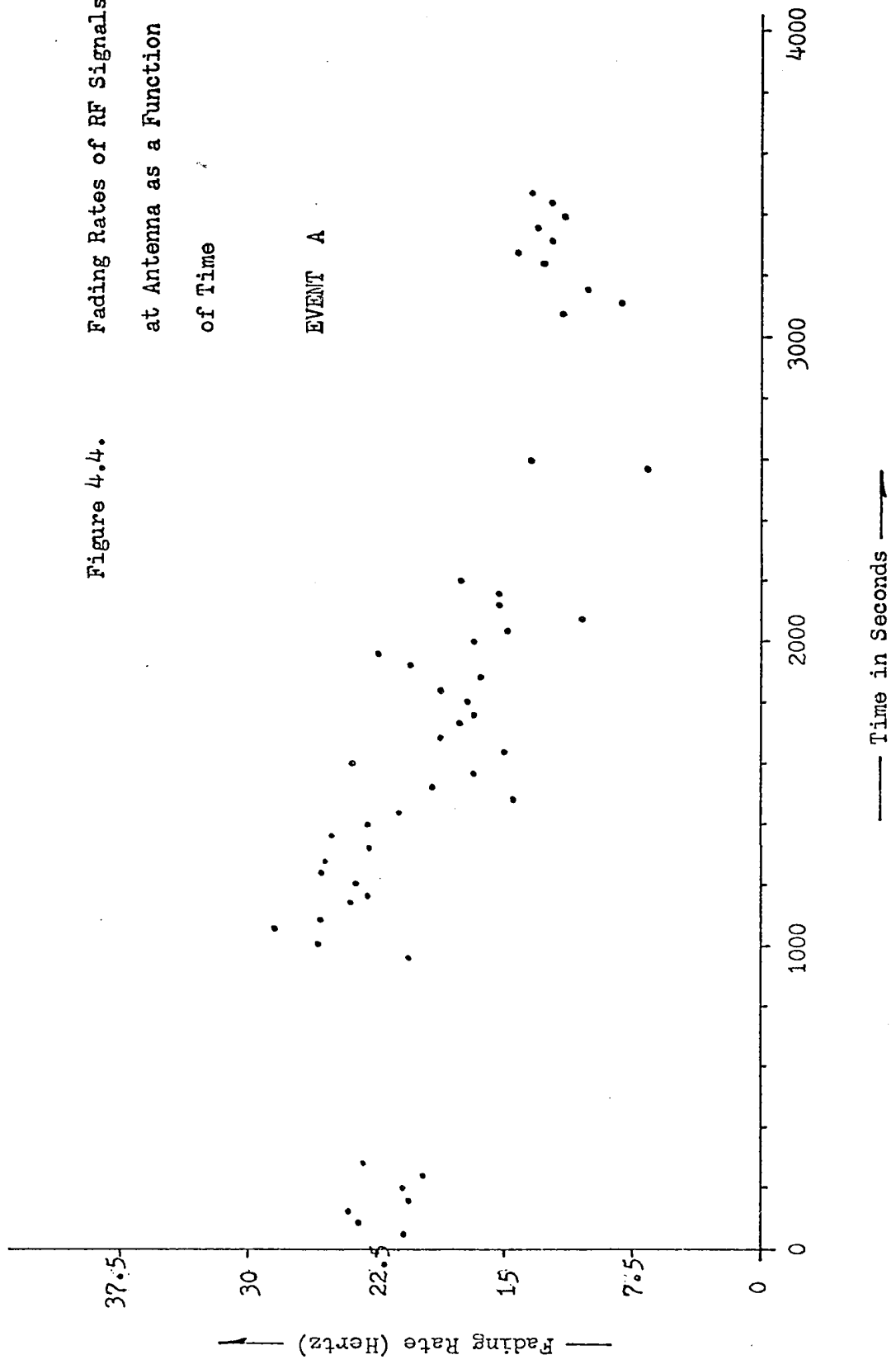
EVENT A

0000 and 0130 UT, December 1, 1966. Its appearance, as recorded on an Esterline - Angus chart recorder, is shown in Fig. 4.5. For this event, 25 forty second samples of signal were analyzed throughout the event. For each sample, the following functions were computed:

a. The temporal autocorrelation functions of the signals received at each antenna. Ideally, all three estimates should be identical. In order to check this, and to give some estimate of the reliability of the results, the three separate comput- ations were carried out. The mean value was used in all calculations.

b. Three sets of crosscorrelation functions corresponding to the three possible antenna separations.

c. The mean amplitude of the signal received at a single antenna during each forty second interval.

The zero-lag crosscorrelation coefficients for the 2λ antenna separation is shown in Fig. 4.6 as a function of time. Because of the greater time resolution available for this event, the fading spectrum width was computed directly from the autocorrelation function width using Eqn. 2.6. As a check, some of these spectrum widths were compared with direct measurements on the spectra (also obtained from ISAC) and were found to be in excellent agreement. The results were then corrected for the finite detector bandwidth and multiplied by $1/\sqrt{2}$ to give the approximate spectral widths of the pre-detected signals. The final results are shown, plotted as a function of time, in Fig. 4.7. The amplitude of the signal, on a linear scale, is shown

EVENT B

Universal Time

Figure 4.5.

Figure 4.6.

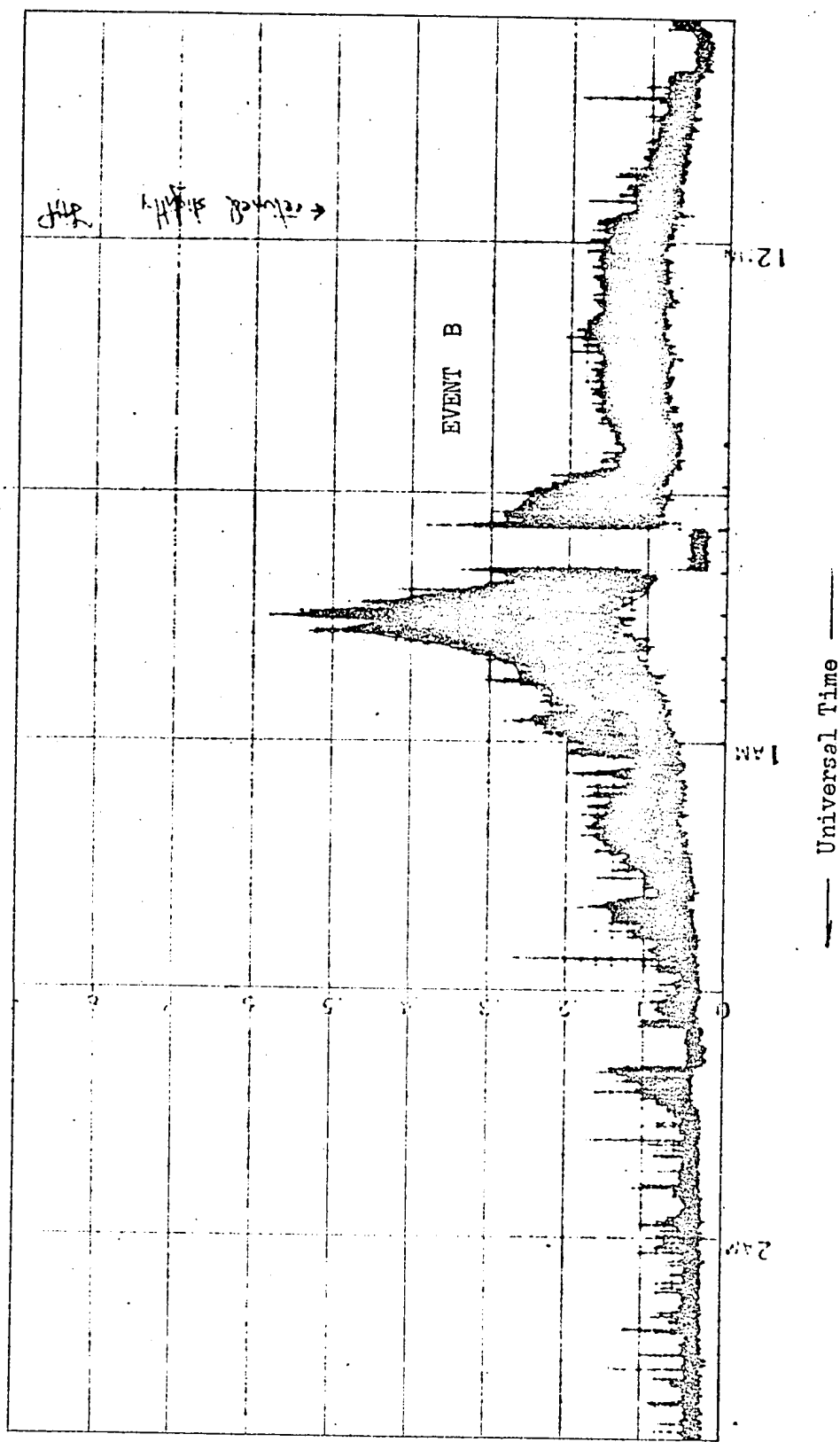Zero-lag Crosscorrelation
Coefficients as a Function
of Time   Event B

Figure 4.7.

Fading Rates of RF Signals
at Antenna as a Function
of Time
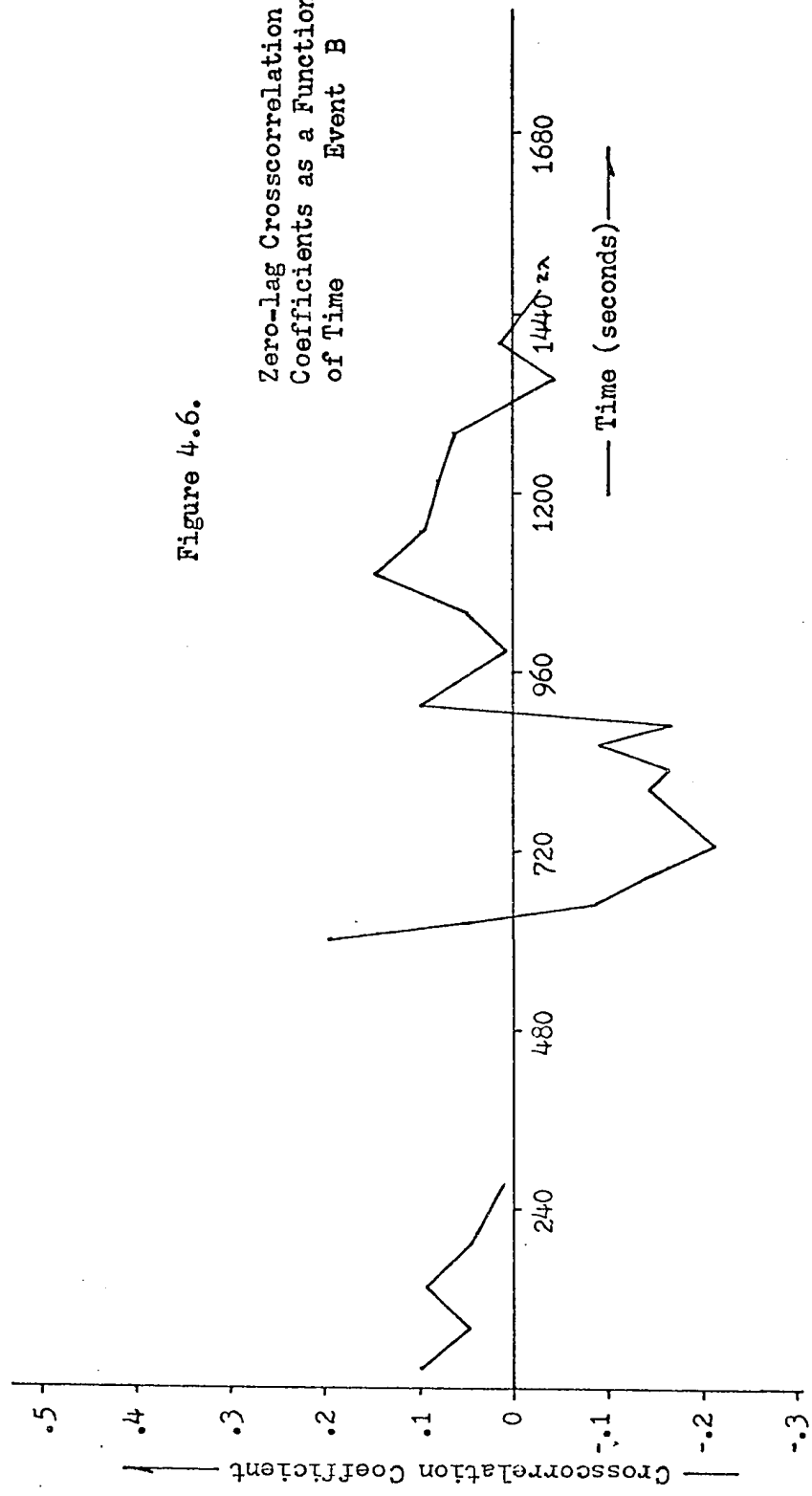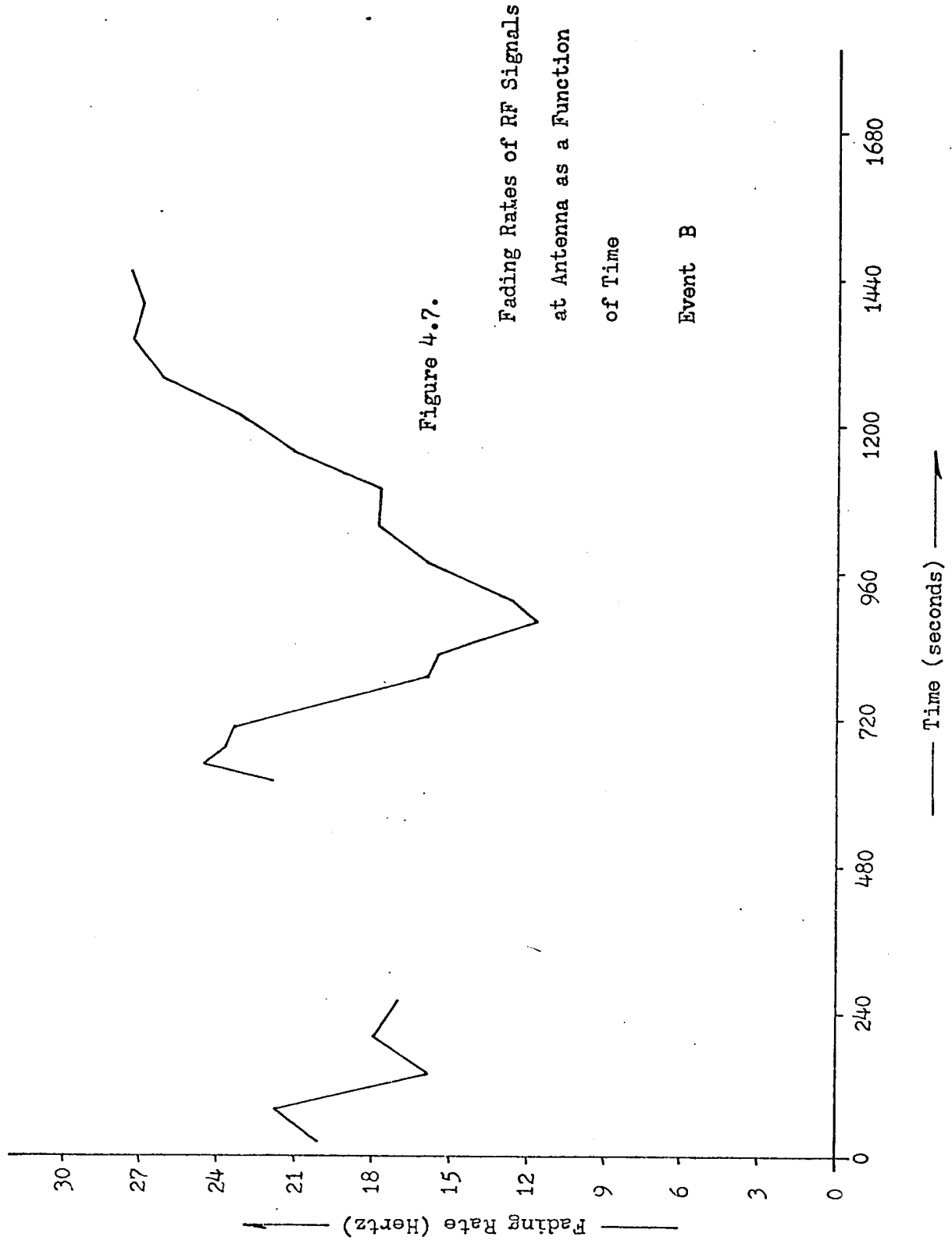
Event B

in Fig. 4.8 as a function of time.

Time displacements were observed on all crosscorrelation functions. These displacements, for each antenna pair, are plotted as a function of time in Fig. 4.9. It is seen that the event may be divided into two distinct phases. In the part of the event coinciding with the period of maximum amplitude, periodicities are evident in both the auto- and crosscorrelation functions. It is useful to plot the time displacements of these functions as a function of antenna separation as in Fig. 4.10. A family of oblique lines is generated whose slope is proportional to the apparent velocity of the amplitude distribution over the ground. Representative examples of the functions themselves are shown in Fig. 4.11. In the remainder of the event, only a single peak is in evidence on the auto- and crosscorrelation functions. Representative auto- and crosscorrelation functions of this region are shown in Fig. 4.12. The transitions from a purely random signal to one with periodic structure, and back again, are quite rapid, taking place in less than one minute. A measure of the abruptness of the change is limited by the forty second time constant introduced by the length of the signal samples used for analysis.

4.3 Event C

This event was recorded on the Ottawa - London circuit between 0400 and 0500 UT, December 1, 1966. The visual appearance of this event, as recorded on an Esterline - Angus chart recorder, is shown in Fig. 4.13. In this case, 48 five second samples of signal were analyzed throughout the event. Auto- and crosscorrelation functions

Figure 4.8.

Amplitude of Event B

as a Function of Time

Time (seconds) ⟶

Amplitude (microvolts) ⟶
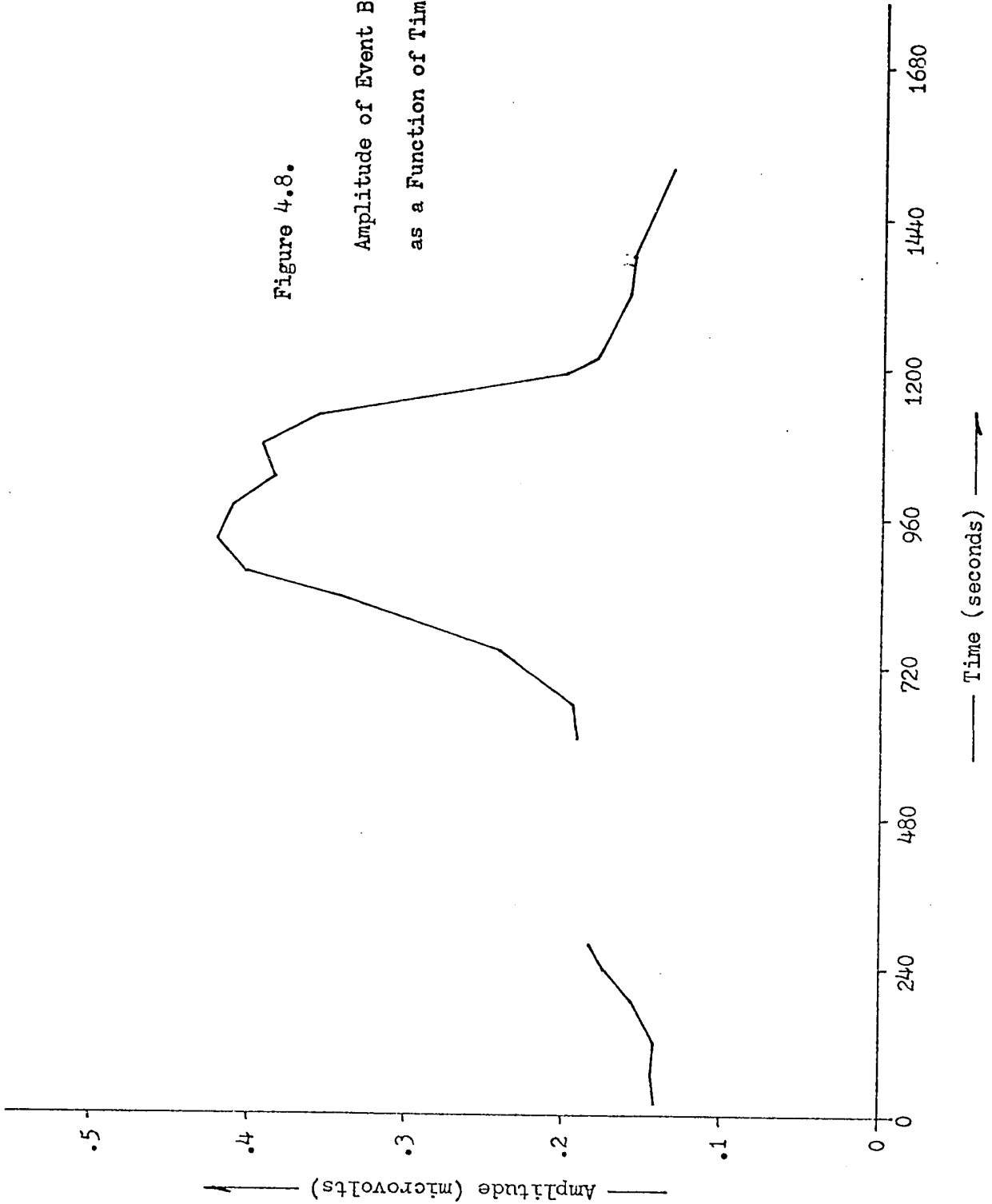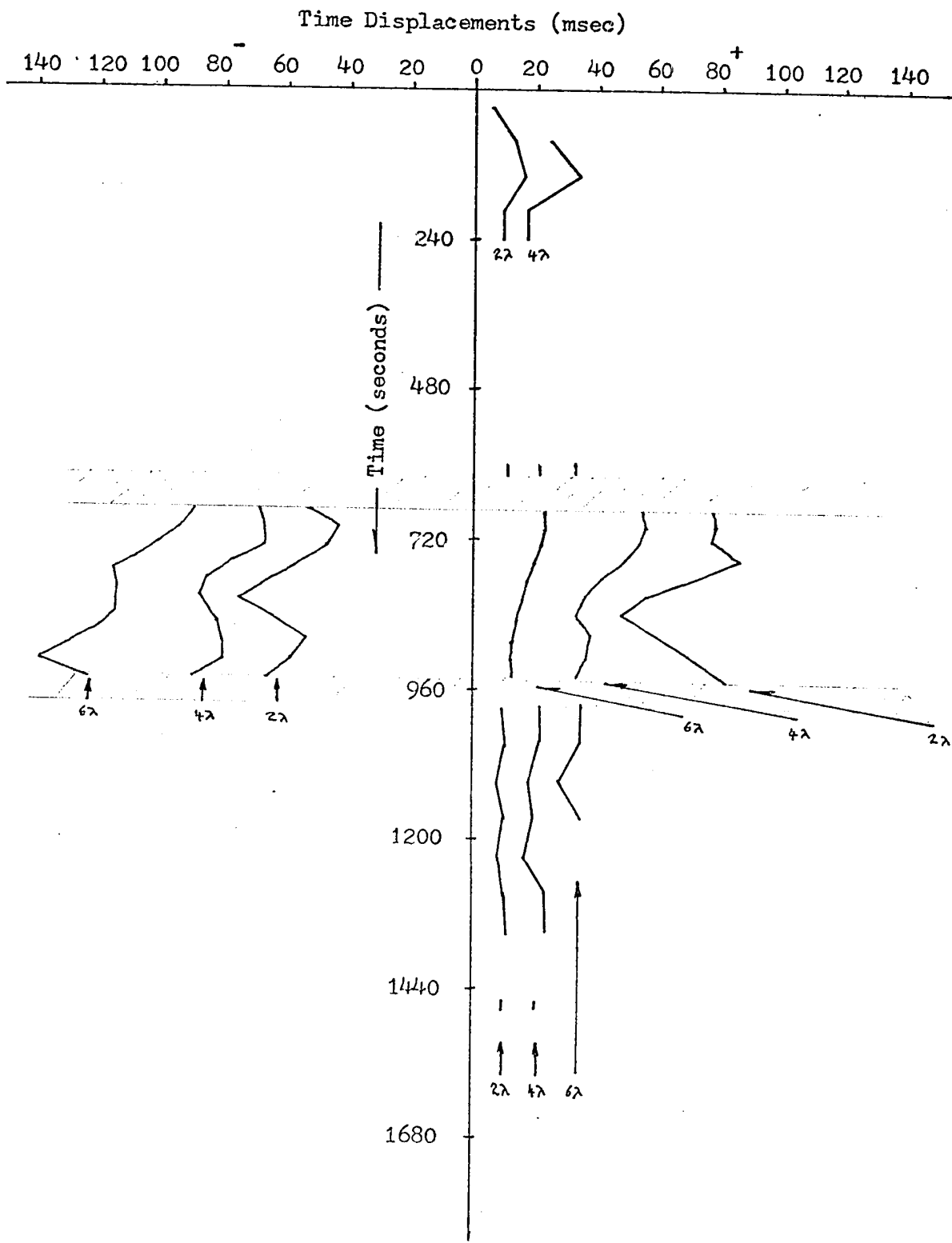
Figure 4.9.

Time Displacements, as a Function of Time, of Peaks
in Crosscorrelation Functions of Event B

Figure 4.10.

Time Displacements, as a Function of Antenna

Separation, of Peaks in Correlation Functions

of Event B

900 - 1100 seconds

Figure 4.11.

Sample Correlation Functions

from Periodic Part of Event B

a. Two wavelength separation Crosscorrelation Function

b. Autocorrelation Function

35
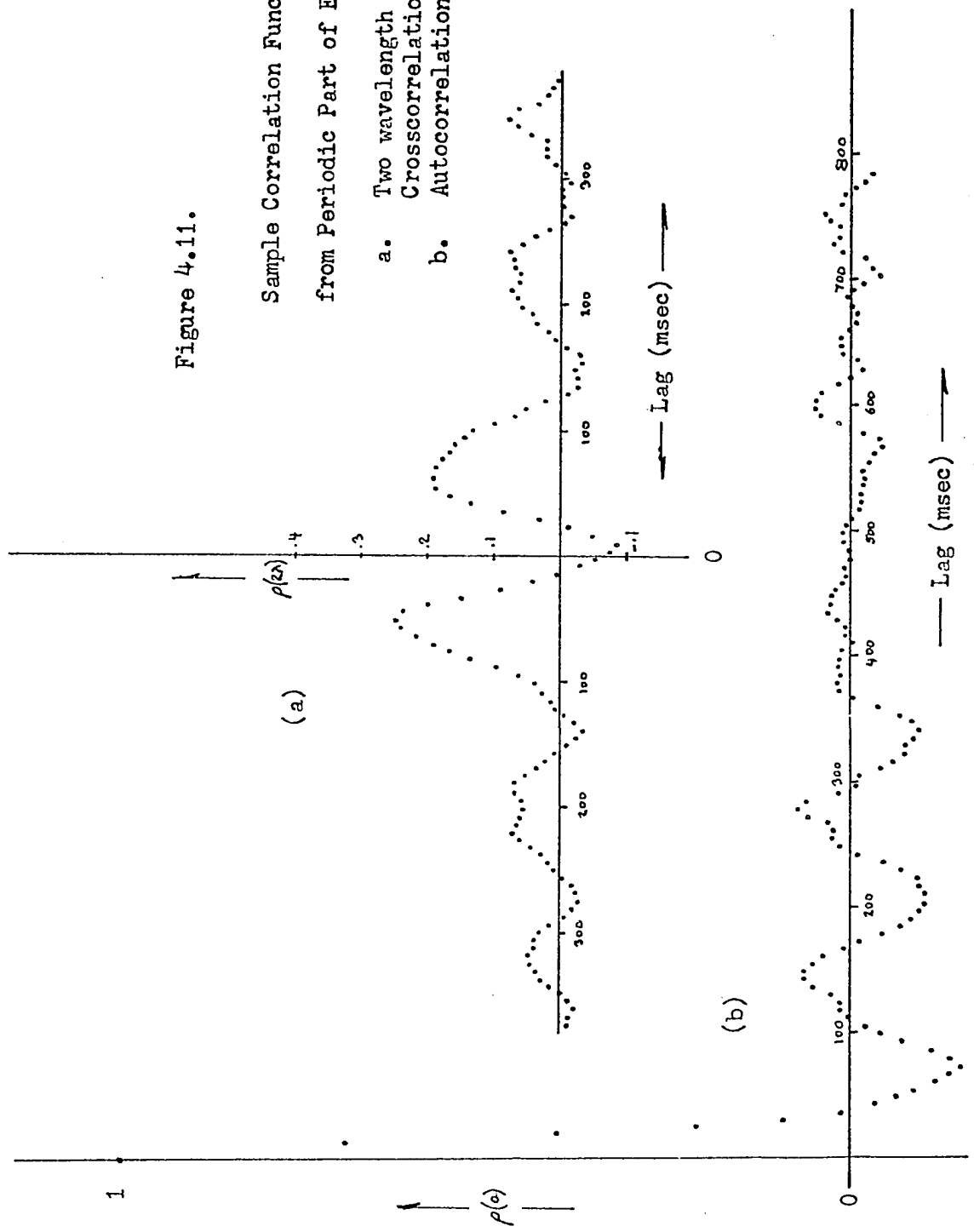
Figure 4.12.

Sample Correlation Functions

from Non-periodic Part of

Event B

a. Two Wavelength separation
   Crosscorrelation Function

b. Autocorrelation Function
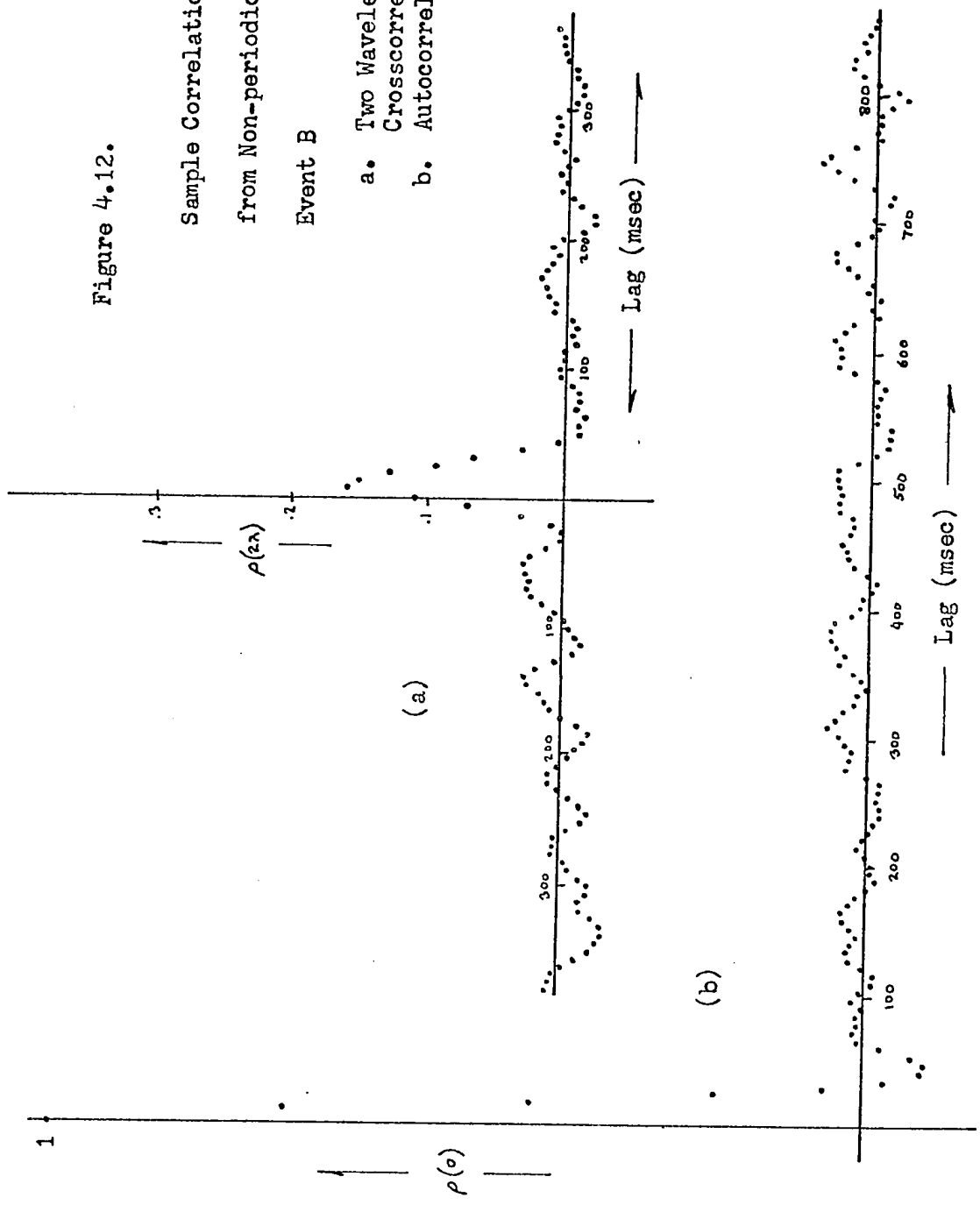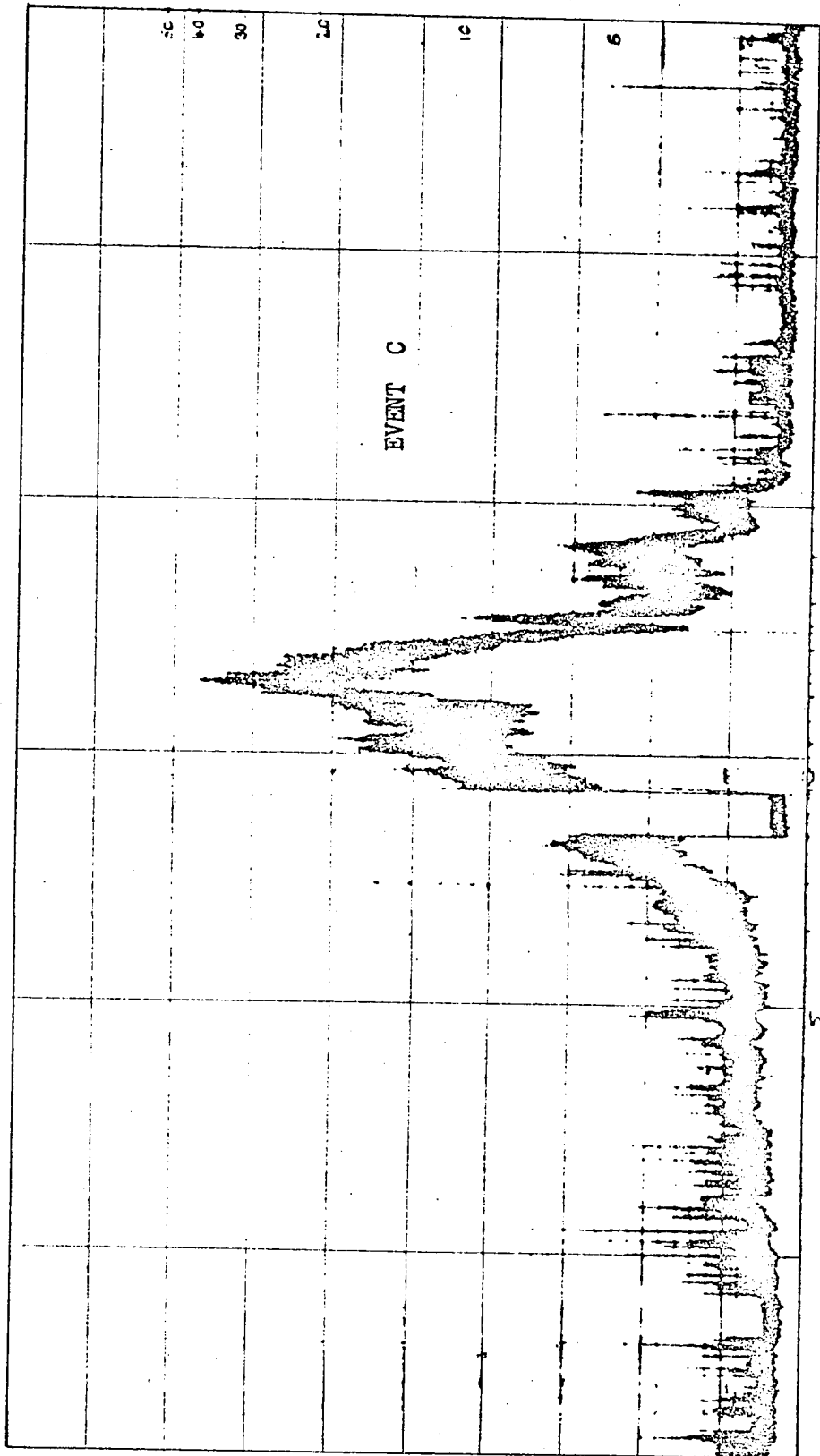
EVENT C

Universal Time

Figure 4.13.

Figure 4.14.

Zero-lag Crosscorrelation

Coefficients as a Function

of Time.   Event C

38
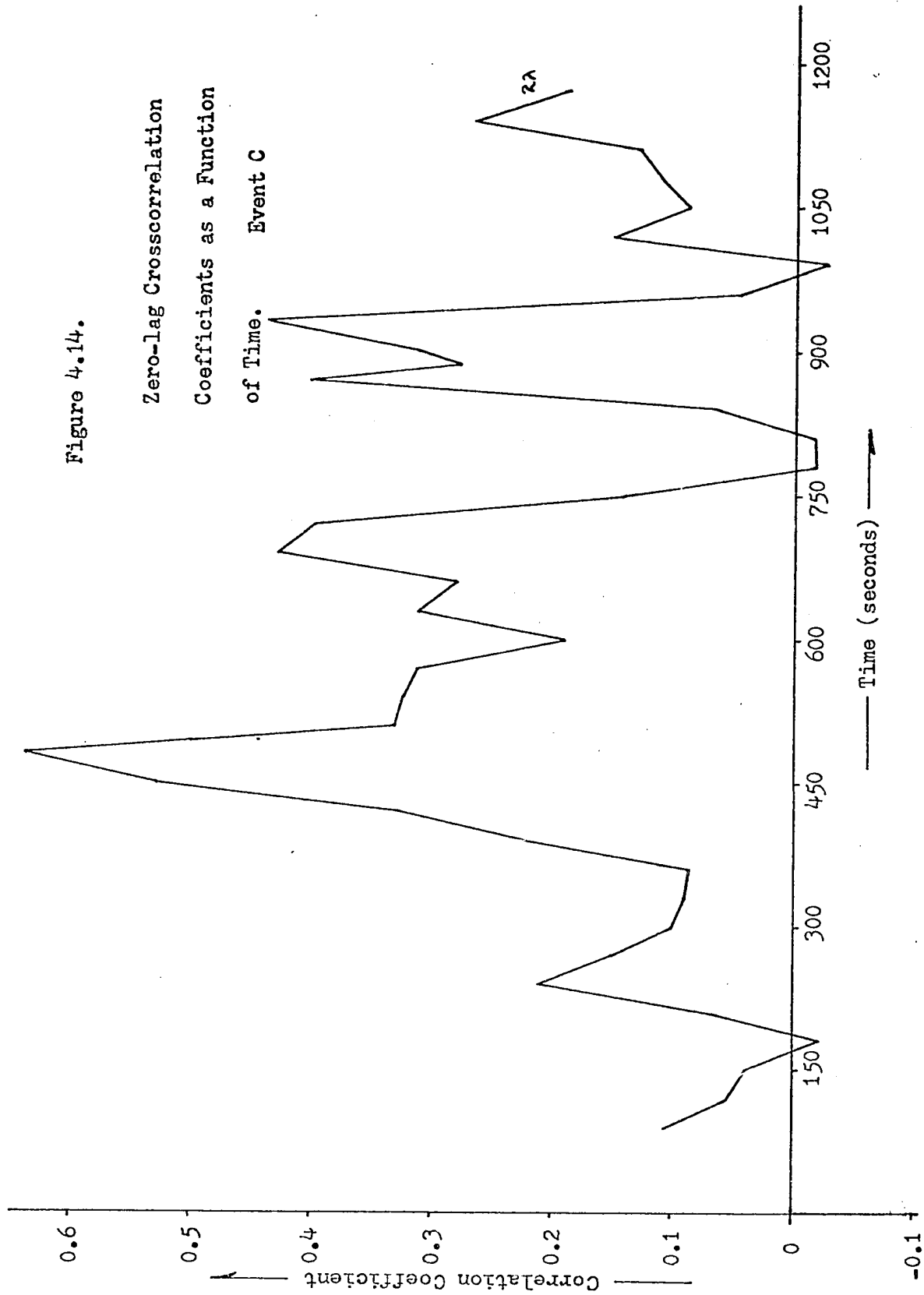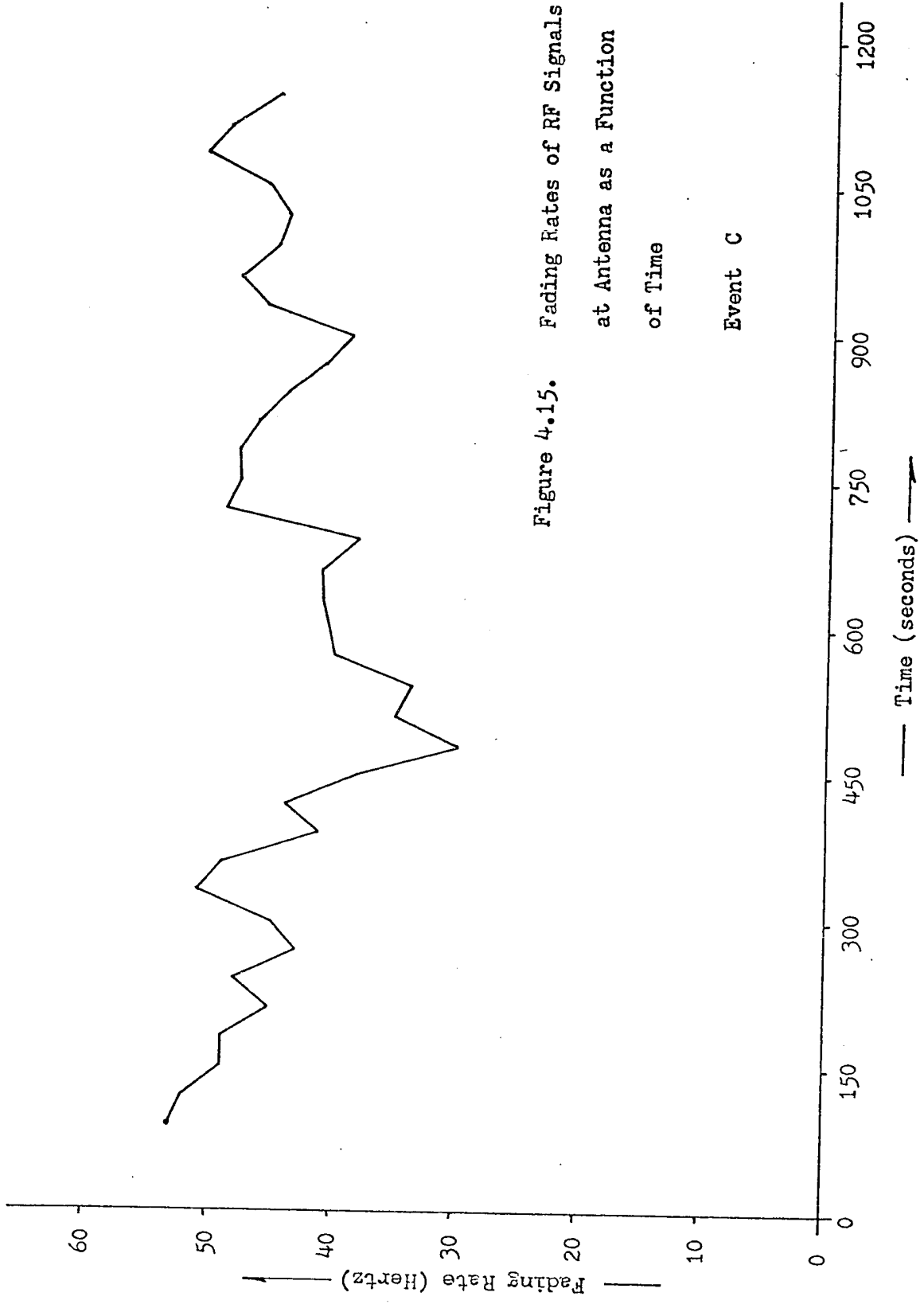
Figure 4.15.   Fading Rates of RF Signals

at Antenna as a Function

of Time

Event C

Figure 4.16

Amplitude of Event C
as a Function of Time
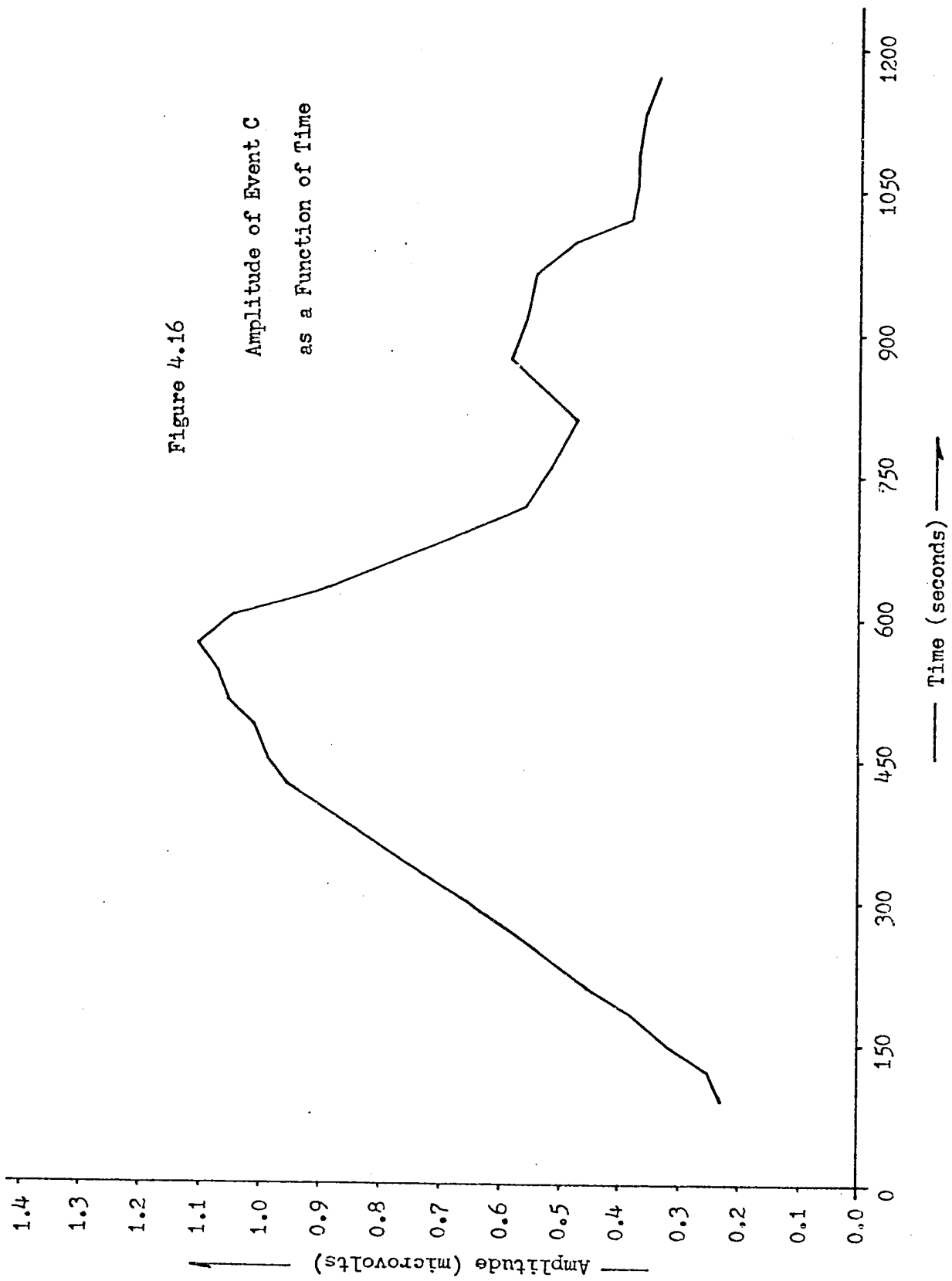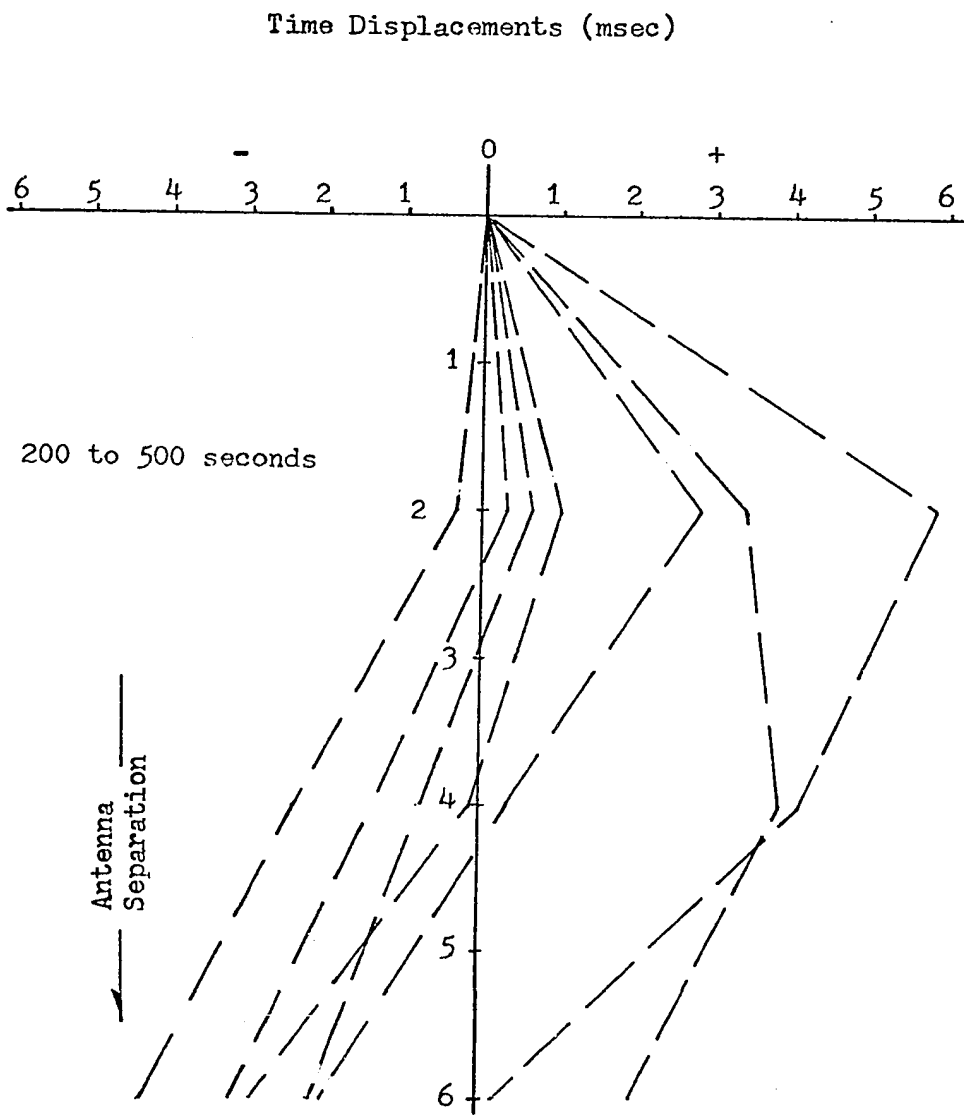
Figure 4.17

Time Displacements, as a Function of Antenna

Separation, of Peaks in Correlation Functions
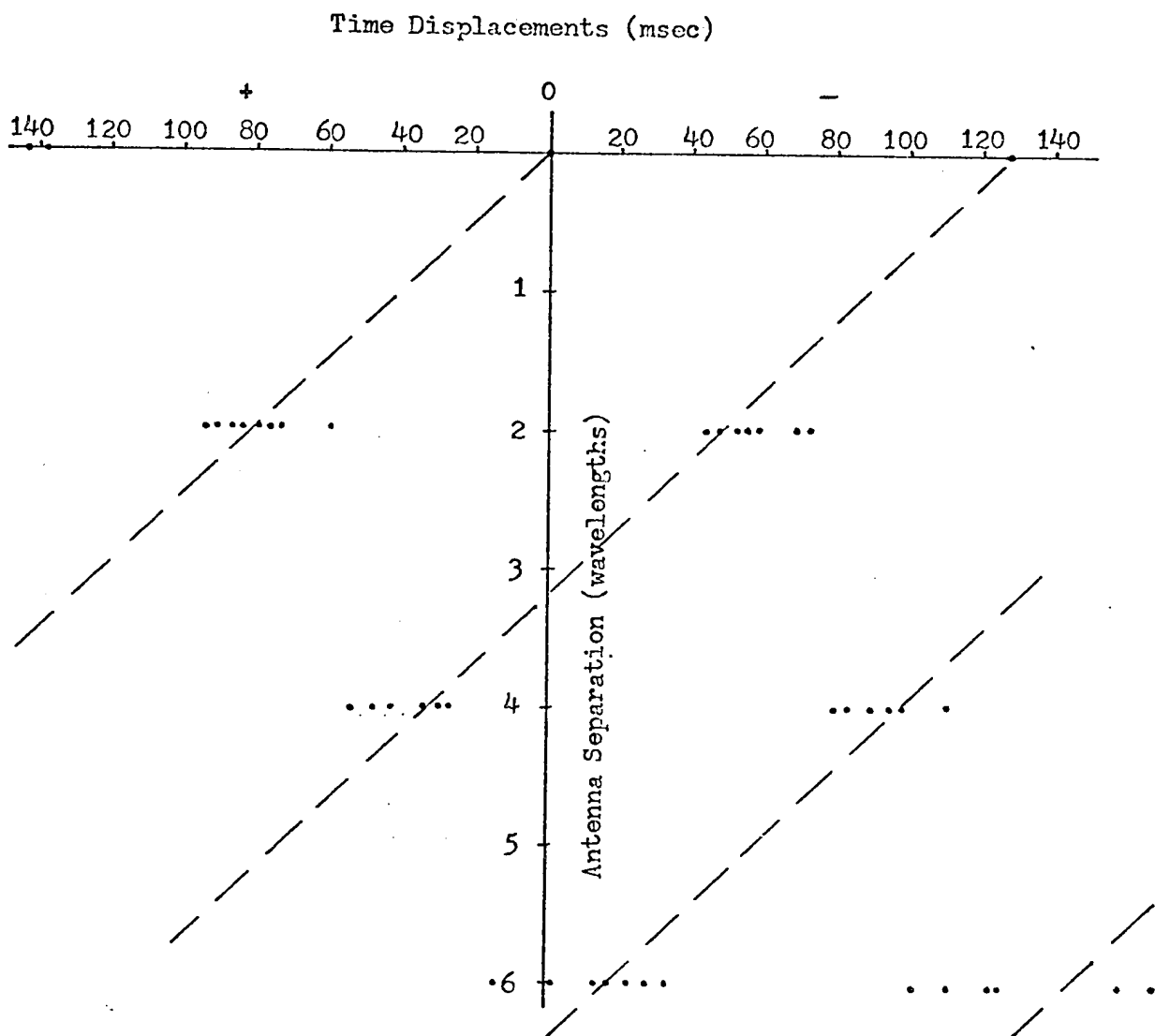
of Event C

Time Displacements (msec)
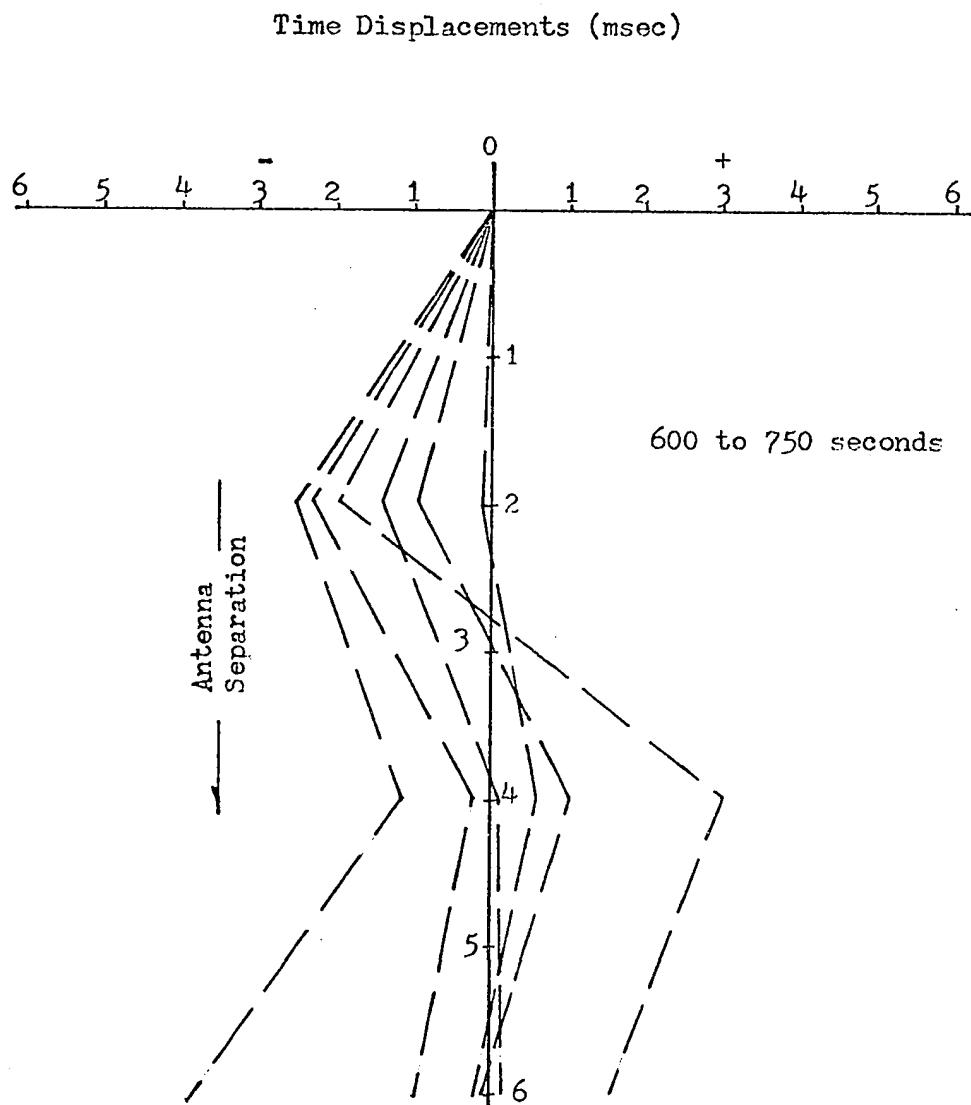
Figure 4.18

Time Displacements, as a Function of Antenna

Separation, of Peaks in Correlation Functions

of Event C

Time Displacements (msec)
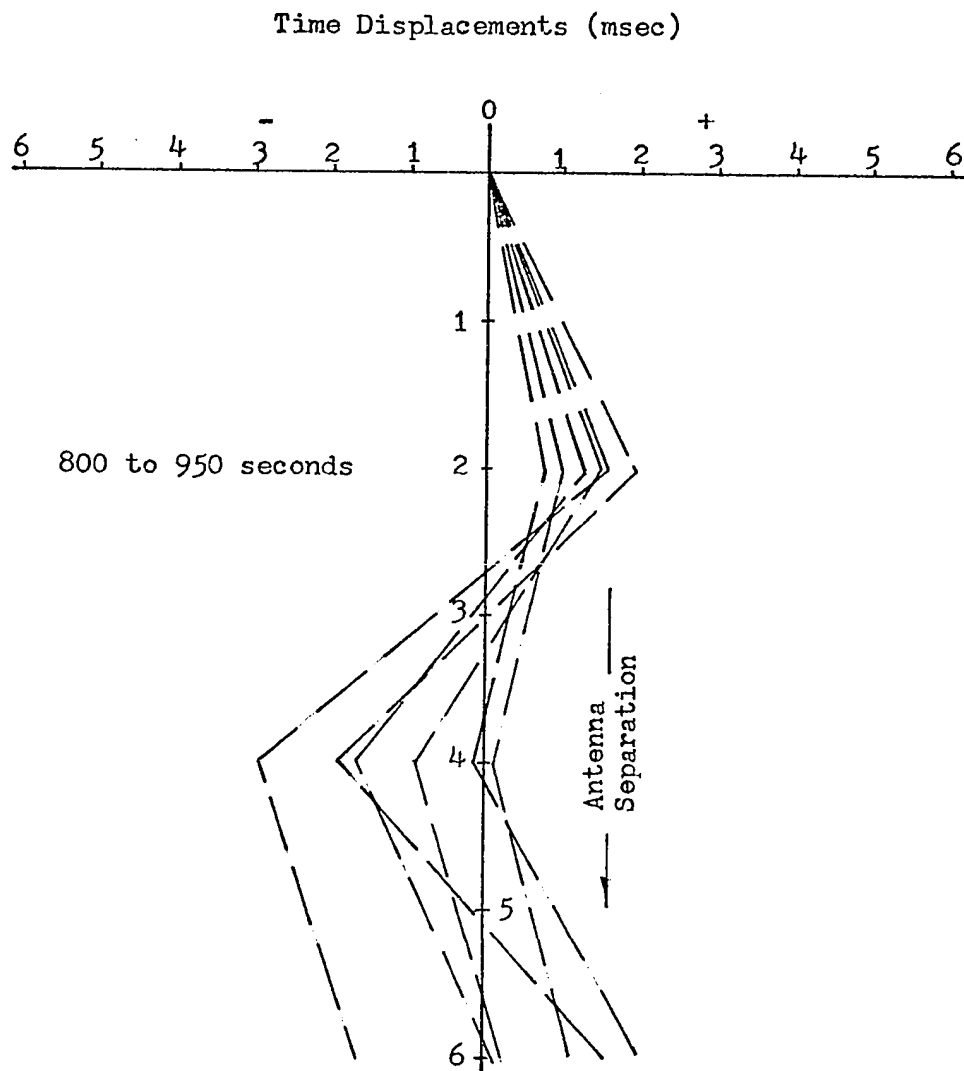
Figure 4.19

Time Displacements, as a Function of Antenna

Separation, of Peaks in Correlation Functions

of Event C

were computed for each segment of signal as in event B. The zero-lag crosscorrelation coefficients for the 2λ antenna spacing are plotted as a function of time in Fig. 4.14. The corrected fading spectrum widths are plotted as a function of time in Fig. 4.15, and the signal amplitude is plotted as a function of time in Fig. 4.16. Time displacements were measureable on all crosscorrelation functions. If such time shifts were due to a drift of the amplitude distribution as a whole, the magnitudes of the shifts would be expected to be in the ratio 2,4,6 for antenna spacings of 2, 4, and 6 wavelengths. In no case was this observed. The magnitudes of the time displacements at different antenna separations appear, at first sight, to bear little relation to one another. They are often of different signs. If correlation function time shifts are plotted as a function of antenna separation for the data of this event, the results shown in Figures 4.17, 4.18, and 4.19 are found. In Appendix B it is shown how the unusual time displacement characteristics shown in these Figures can be simulated by the superposition of fields scattered from more than one region.

CHAPTER V

CHARACTERISTICS OF THE DIFFRACTION PATTERNS

5.1 Spatial Autocorrelation Functions and Scale Sizes

The scale sizes of the diffraction patterns on the ground, in the
direction of the line joining the antennas, may be found from a plot
of the zero-lag crosscorrelation coefficients as a function of distance
(antenna spacing). As previously mentioned, the appropriate cross-
correlation coefficients are the square roots of the measured ones.
Such a plot is equivalent to the spatial autocorrelation function of
the diffraction pattern. Scale size may be determined from a single
crosscorrelation coefficient measurement of the nature if the spatial
variation is assumed. In previous work a gaussian spatial auto-
correlation function has usually been assumed, and this is done in
the case of event A. Estimates of scale size, as a function of time,
are shown for event A in Fig. 5.1. Of great interest are the very
large scale sizes computed for the latter half of this event.

Inspection of the spatial autocorrelation functions computed for
events B and C will show that the assumption of a gaussian envelope is
not always justifiable. These functions are shown plotted as a function
of time in Figs. 5.2 and 5.3 respectively. Non-gaussian examples.
of spatial autocorrelation functions are shown in Fig. 5.4. These,

Figure 5.1   Scale Size as a Function
              of Time
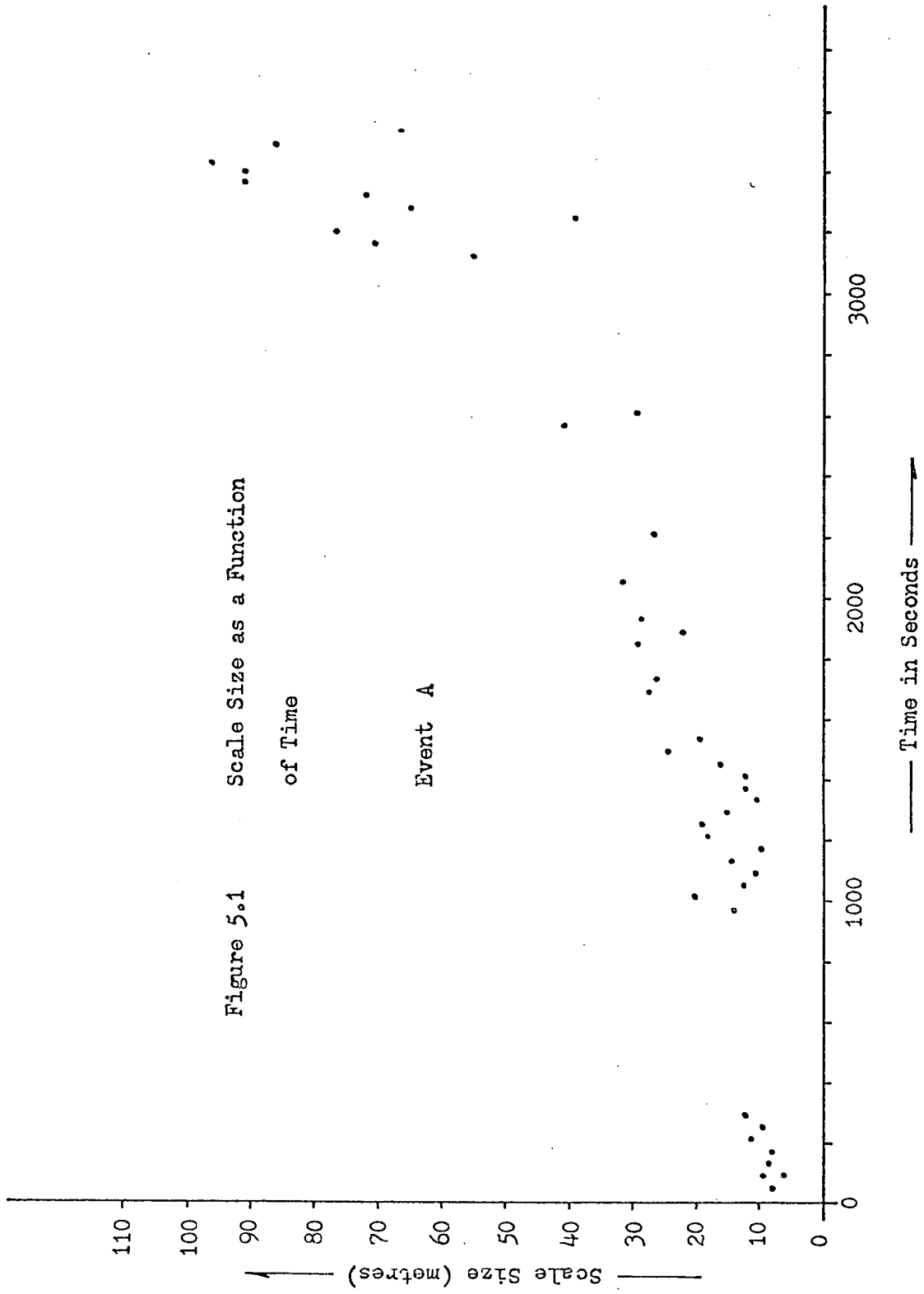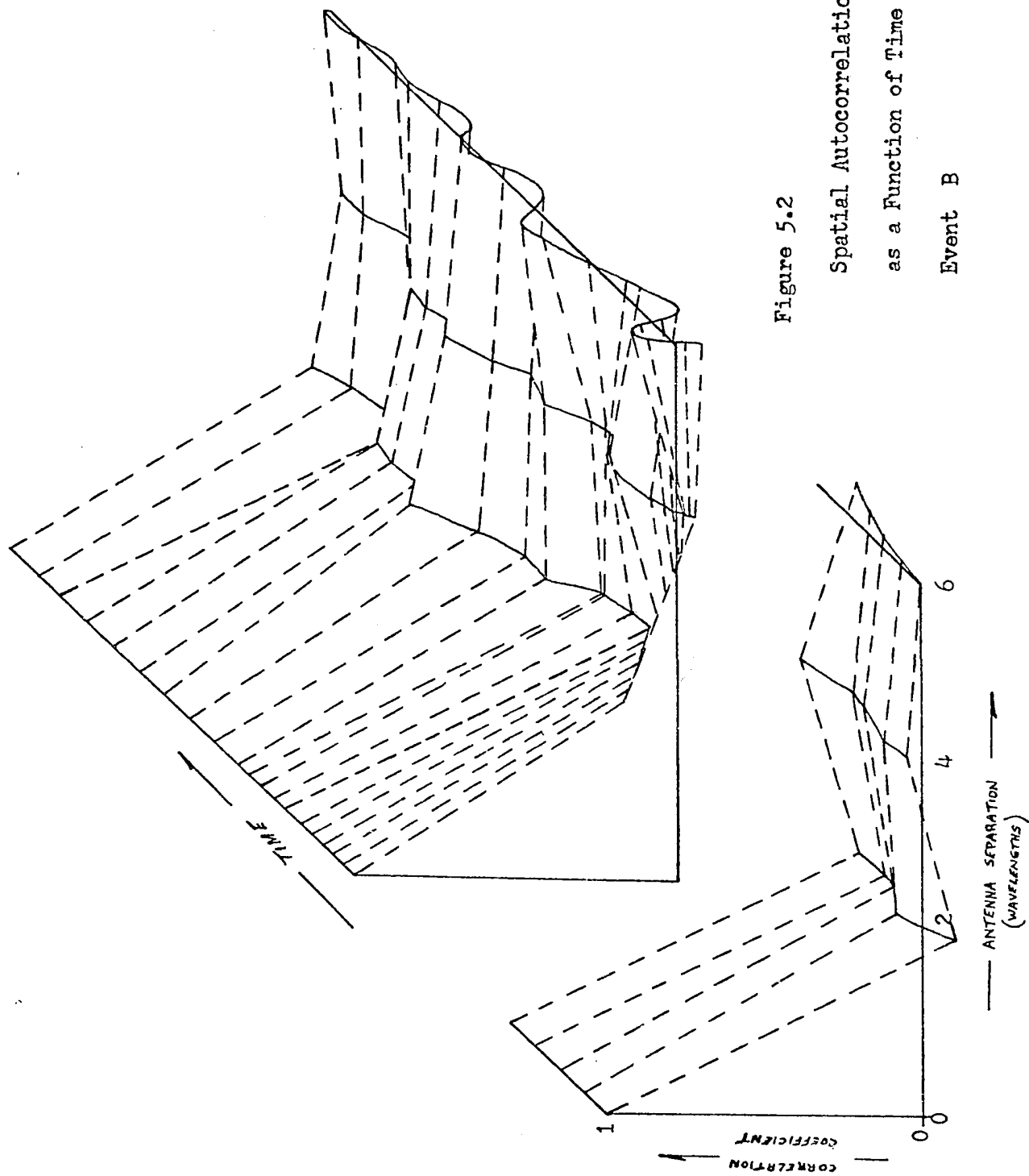
              Event A

Figure 5.2

Spatial Autocorrelation Functions

as a Function of Time

Event B

Figure 5.3

Spatial Autocorrelation
Functions as a Function
of Time
Event C
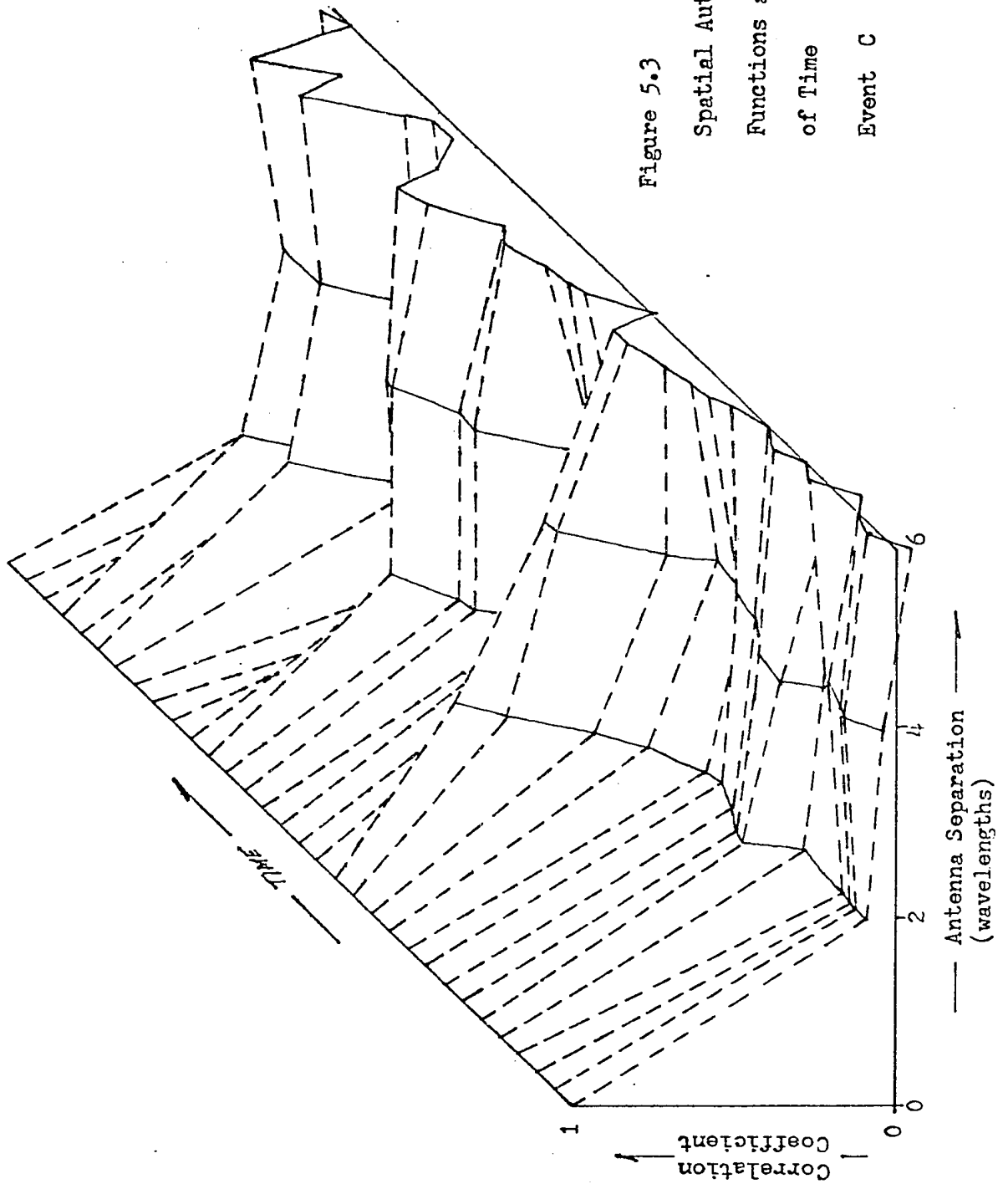
Figure 5.4   Representative Spatial Auto-
Correlation Functions.

Event B
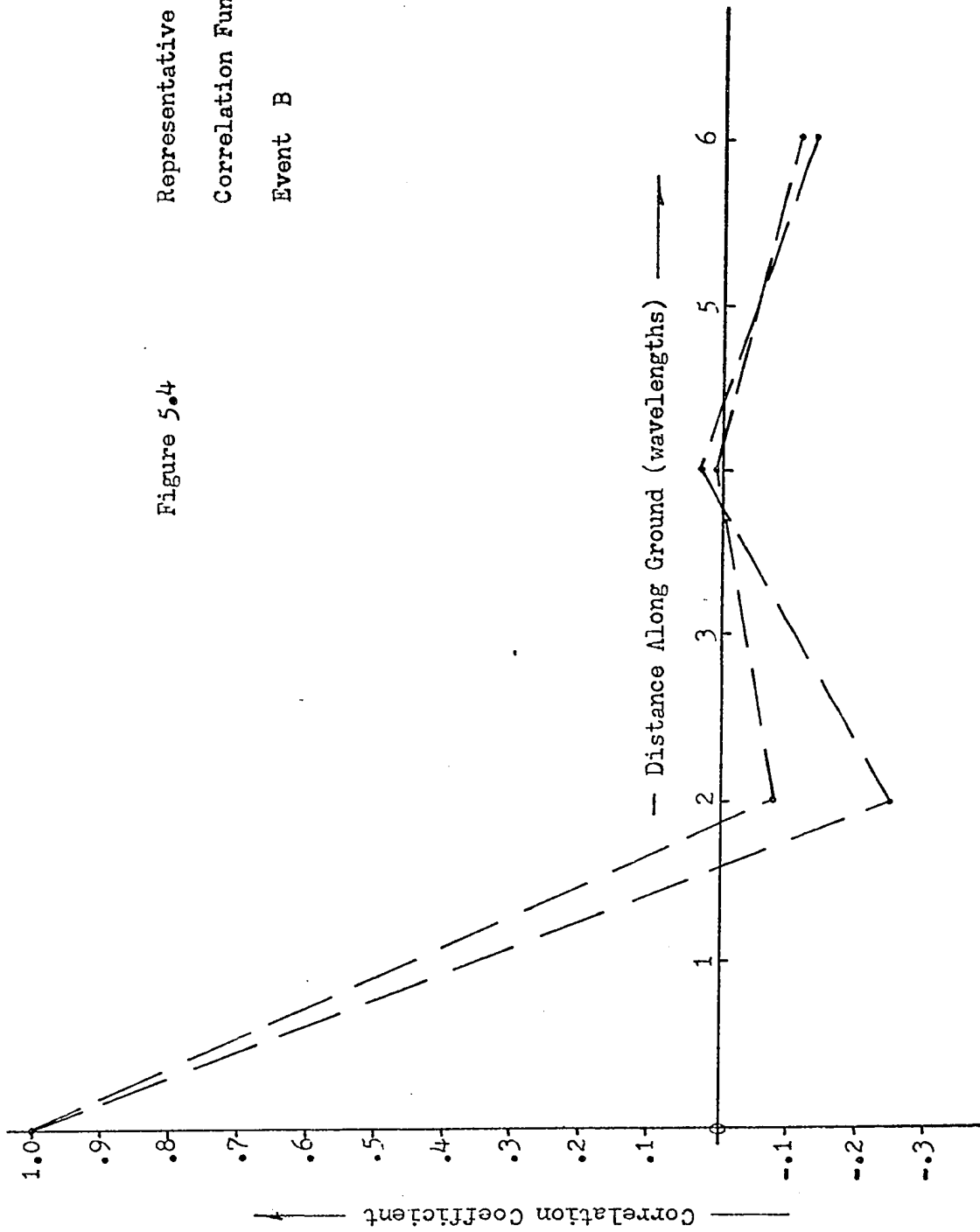
taken from event B, are quasi-periodic in nature. It is seen that the scale size of the structure in the non-periodic part of event B is at all times comparable with the transmitted wavelength.

The forms of the correlation functions in event C range from approximately gaussian (specific examples of which are shown in Fig. 5.5) to definitely non-gaussian (examples of which are shown in Fig. 5.6). As for event A, scale sizes range from near the wavelength used to approximately 100 metres.

The implications of the results presented here will be discussed in Chapter Six.

5.2 Diffraction Pattern Velocities

The derivation of the velocity and rate of change of the diffraction pattern of the RF field on the ground at the receiving site is carried out using the theory developed by Briggs et al., (1950), and by Phillips and Spencer (1955). Their work was carried out primarily for use in interpreting the results of vertical incidence sounding experiments. It is also applicable to the case of oblique scatter with little modification. Vertical incidence measurements are generally made at three antennas which form the vertices of a right angle triangle. In this way, velocity components in two directions are available, thus enabling the true velocity of the pattern to be determined. The question which arises now is how much can be said concerning the nature of the velocity vectors when measurements in only one dimension are available. It is first necessary to make a number of definitions (following Briggs et al., 1950).

Figure 5.5   Representative Spatial Auto-

Correlation Functions.
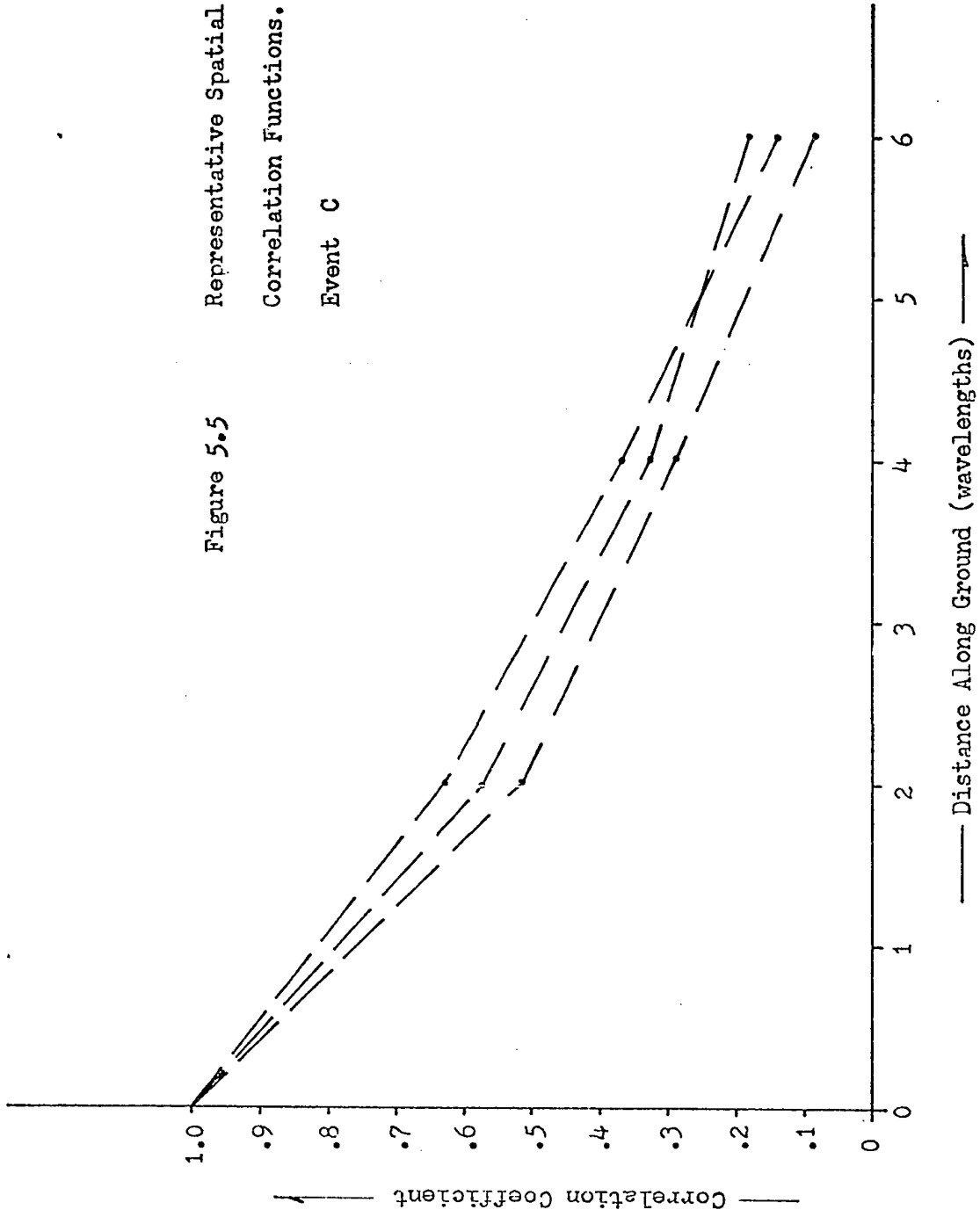
Event C

Figure 5.6.

Representative Spatial Auto-
Correlation Functions.
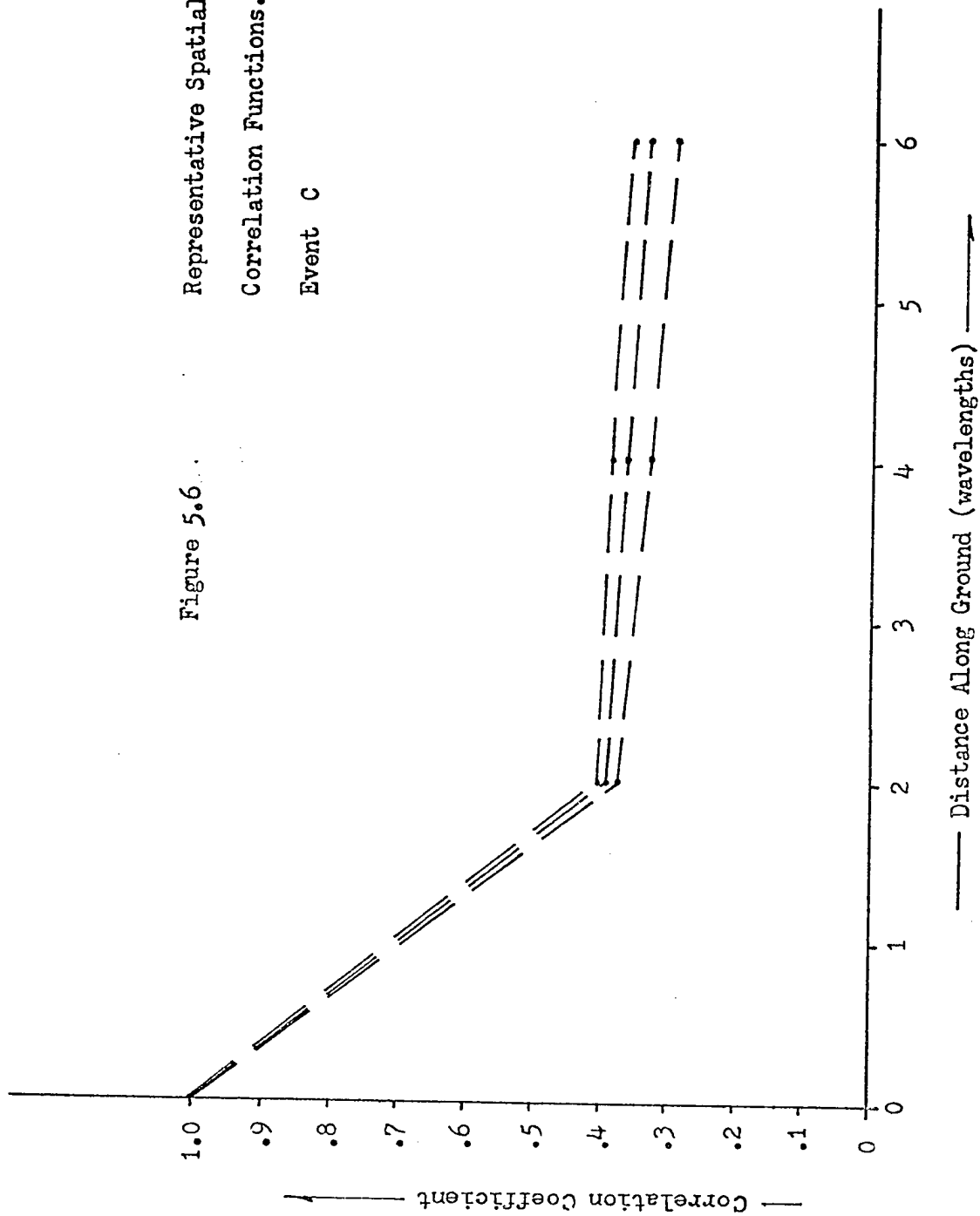
Event C

V Actual velocity of the diffraction pattern over the ground.

V' Apparent velocity of the diffraction pattern between two spaced antennas, as measured from crosscorrelation function time displacements.

V'_c Velocity an unchanging diffraction pattern would need in order to give the observed fading rate. $V'_c = \xi_0/\tau_0$ where ξ_0 (antenna separation) and τ_0 satisfy the relation

$$\rho(\xi_0, 0) = \rho(0, \tau_0) \qquad\qquad 5.1$$

V_c V'_c as measured by an observer moving at the velocity V. V_c gives a measure of the rate of change of the diffraction pattern with time.

Subscripts t and l will refer to the transverse and longitudinal components of the above variables, with respect to the expected direction of arrival of the scatter signals. This direction is at right angles to the line joining the antennas.

Limits are derived in Appendix A for the possible values of V and V_c in terms of the measured values of V'_t and $(V'_c)_t$. The results are

$$\frac{(V'_c)_t^2}{V'_t} \leq V \leq V'_t \qquad\qquad 5.2$$

and

$$0 \leq V_c \leq (V'_c)_t \left(1 - \frac{(V'_c)_t^2}{(V'_t)^2}\right)^{\frac{1}{2}} \qquad\qquad 5.3$$

Event A:

$(V'_c)_t$ was computed for each signal sample using Eqn. 5.1. This was done using the two autocorrelation functions and the mean was used. In order to find bounds for the true drift velocity V an

estimate of V_t' is needed. There is no case in the records of a time shift between the two signals greater than 2.5 msec. This could be taken as indicating that either

      a. $V_t' \sim 0$

or   b. $V_t' \geq 6,000$ m/sec.

Possibility (a) may be eliminated since it implies, by Eqn. 5.2, that V is undefined and the lower bound approaches infinity. This is not admissable since V_t' must be greater than, or equal to, V. Case (b) is the only alternative. Using this value of 6,000 m/sec., a lower bound may be placed on V, using the expression 5.2. Since V_t' is not known, this represents only an upper limit to the lower bound. Bounds may be placed on the fading velocity, V_c, of the signal by using Eqn. 5.3, even though V_t' is not known.

    Both of the above sets of bounds are shown, plotted as a function of time, in Fig. 5.7.

Event B:

    Three antennas were used in recording this event. Also, a higher time resolution was used in analyzing the data than in case A. In this case also, $(V_c')_t$ was found as a function of time. As may be seen from the plot of time displacements as a function of time in Fig. 4.9, this event exhibits rather different behaviour than did event A. In this case there are very definite and compatible time shifts indicated in the crosscorrelation functions computed for different antenna separations. For the two non-periodic parts of the event, the time shifts are compatible with an

Figure 5.7. Approximate Lower Bounds on V

and Upper Bounds on V_c.

Event A

- = V

x = V_c

Velocity (m/sec)

— Time (seconds) —
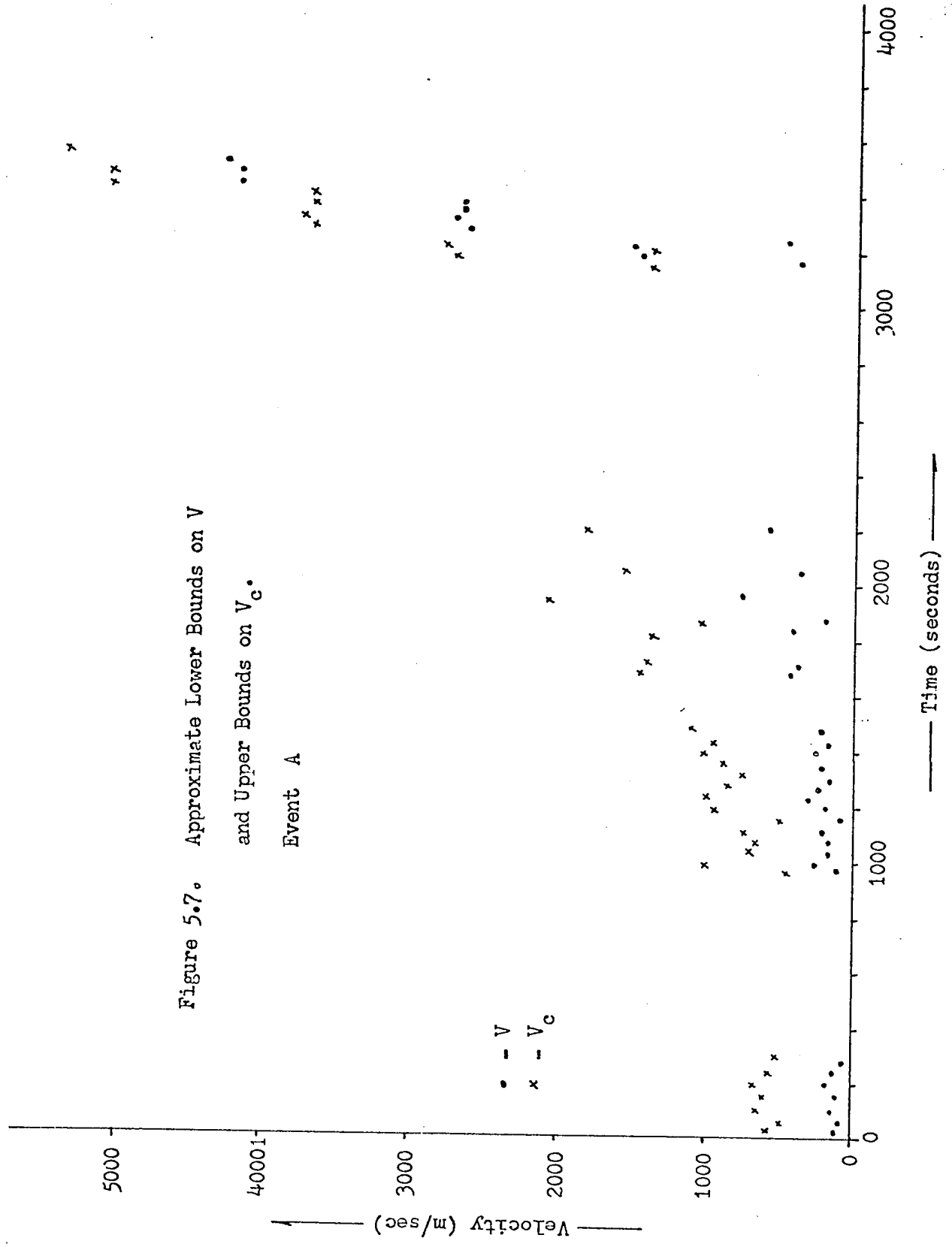
apparent east to west transverse drift velocity of approximately 1600 m/sec. In this case, both upper and lower bounds can be placed on the possible values of both V and V_c. Bounds on V for the non-periodic parts of the event are plotted as a function of time in Fig. 5.8.

In the periodic part of the event, both the auto- and cross-correlation functions have periods of approximately 132 msec. The spatial autocorrelation functions indicate a spatial wavelength of approximately 4 wavelengths or 30 metres. It is easy to check whether the periodic fading is due to motion of periodic structure across the ground or whether it is due to a periodic temporal variation in the signal amplitude. If the former is true, the crosscorrelation function time displacements should change uniformly with antenna separation, whereas in the latter case the time displacements should be independent of antenna separation. Reference to Fig. 4.10 will show that the time displacements change uniformly with antenna separation and so it is inferred that the periodic fading is produced by the drift of the periodic structure across the ground. The spatial wavelength of the structure may be determined from the antenna separation at which oblique lines, drawn through the experi-mental points, cut the vertical axis. Drift direction is determined by noting, from Fig. 5.4, that a peak in the spatial autocorrelation function occurs at an antenna separation of between 2 and 6λ. In order to have a peak occur in this range in Fig. 4.10 an east to west drift must be assumed. Fig. 4.10 then gives the spatial wavelength of the structure as $3\frac{1}{4}$ times the transmitted wavelength, and the apparent drift velocity as approximately 200 m/sec.

Figure 5.8. Bounds on Possible Drift

Velocities: Event B
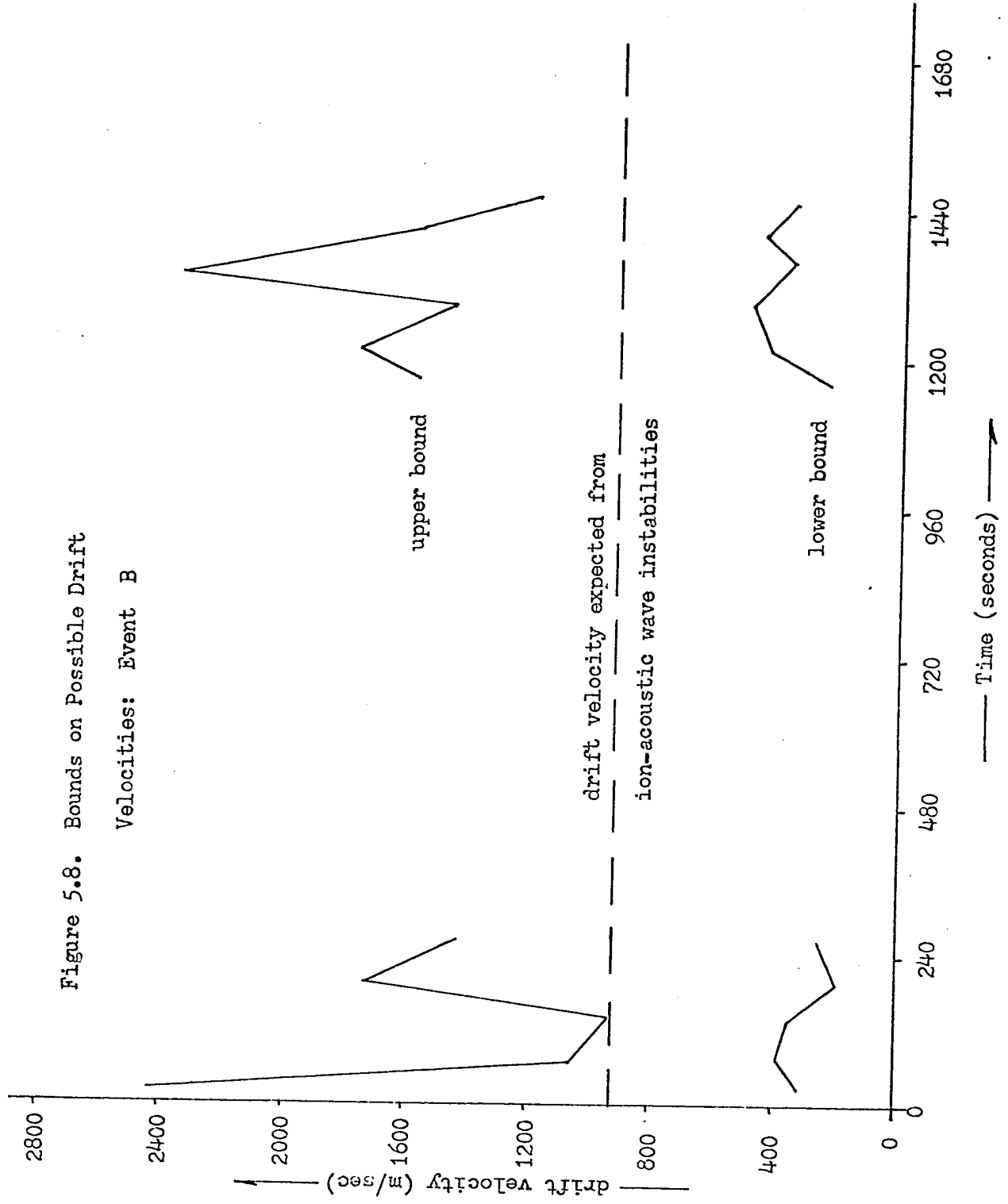
If a mean fading period of 132 msec is assumed, it is easily shown, since $V = f\lambda$, that the transverse component of the apparent drift velocity is approximately 200 to 228 m/sec. Substitution of experimental values into Eqn. 5.2 shows that the true drift velocity V of the periodic structure must be close to the experimental value of V_t' : 200 to 228 m/sec. V_c can be shown to be approximately zero, by Eqn. 5.3, throughout most of this part of the event.

Event C:

The details of the recording and analysis of this event are the same as for event B. $(V_c')_t$ was found to be almost constant at 2.4 km/sec as a function of time. In order to place bounds upon V and V_c we need an estimate of the magnitudes of the time shifts of the cross-correlation functions. As mentioned, time shifts were measureable, but were not consistent with the idea of a single drifting diffraction pattern. It is shown in Appendix B that the observations may be interpreted as being due to the superposition of two or more diffraction patterns on the ground; each pattern having a different velocity and spatial correlation function. Approximations to the apparent velocities of each region may be found from the plots of cross-correlation function time displacements as a function of antenna separation. Such plots for event C have been shown in Chapter Four. Velocity components in both easterly and westerly directions are observed. Typical bounds for the drift velocities V, of the diffraction patterns due to each region, are calculated to be approximately 0.5 to 10 Km/sec. The corresponding values of the fading velocity V_c

range from zero to 0.5 Km/sec. The observed fading is thus primarily
due to drift of the diffraction pattern over the ground rather than
to change of the diffraction pattern with time.

CHAPTER VI

INTERPRETATION OF THE RESULTS

Before embarking on a discussion of the results of Chapter Four in terms of possible scattering mechanisms, it is first necessary to examine in detail the nature of the diffraction pattern to be expected from scattering regions in general.

6.1 Scattered Fields in General

Consider first a scattering region of infinite lateral extent containing a random array of scatterers. It appears obvious that the spatial correlation function of the amplitude fluctuations on the ground is related in some way to the properties of the irregularities in the ionosphere. Here we wish to show that the usual interpretation (Ratcliffe, 1956), which is applicable to radio-star, satellite, and vertical-incidence-sounder observations of the ionosphere does not apply to observations on scatter circuits, except in very special circumstances.

It can be shown that in the radio-star and satellite measurements, which are carried out at sufficiently high frequencies that reflections and effects due to multiple scattering are unimportant, that the scale size of the structure on the ground is given by

$$L = L^*/\Delta\Phi \text{ if } \Delta\Phi > 1 \quad \text{and } L = L^* \text{ if } \Delta\Phi \ll 1 \qquad 6.1$$

where L* is the scale size of the structure in the ionosphere and

$\Delta\Phi$ is the maximum phase deviation of the wavefront after passing

through the ionosphere. It is usually assumed that at the frequencies

used, $\Delta\Phi$ is small so that L = L*. When lower-frequency, ground-based

transmitters are used for vertical-incidence sounding, it is usually

assumed that the reflection takes place in a very thin stratum com-

pared to the wavelength used so that the phase deviations are small

and the scale size of the structure on the ground is again nearly that

of the irregularities themselves.

The interpretation of obliquely scattered signals is very diff-

erent. As for the vertical incidence soundings, the direct transmitted

wave is not available at the receiver. Since the radio waves are

scattered through large angles from all points within the scattering

volume, the relative phase differences between the various wavelets

scattered in the direction of the receiver can be extremely large,

limited only by the overall depth of the scattering region. Because

of the wide angular spectrum of the scattered field from such a region,

the amplitude structure of the diffraction pattern is fully developed

beyond only a short distance from the scattering region, and the first

part of Eqn. 6.1 holds well. The scale size of the structure on the

ground is thus a small fraction of the scale size of the individual

scatterers themselves. For example, if the scattering region is only

250 wavelengths thick, the phase deviations of an obliquely emerging

wavefront can be as large as 1000 π radians. This will result in

structure on the ground which is 1/1000 π as large as that in the

scattering region itself. It has been shown elsewhere (cf. Booker, 1960)

that if the auroral echoes in the VHF band are to be interpreted in terms of weak scattering the irregularities must have dimensions comparable to the wavelength of the transmitted signal. For any scattering volume more than a few wavelengths thick then, the scale size of the diffraction pattern on the ground is extremely small, and the minimum size is limited only by the wavelength used.

The deduction of ionospheric scale sizes from forward scatter records has previously been carried out in a manner similar to that used in the case of radio stars, since the geometry of the problem is, at first sight, quite similar. In this case also, it is easy to show that the scale size of the structure on the ground is but a fraction of the scale size of the scatterers themselves, although the effect is not as extreme as in the case of oblique scatter. The magnitude of the maximum phase deviation $\Delta \Phi$, may be estimated by the construction of appropriate Fresnel zones, as indicated in Fig. 6.1.

Fresnel Zones on

Forward Scatter Circuit

FRESNEL ZONES

25 M

2.5 KM

100 KM

HORIZON

T ↓ R (line joining transmitter and receiver)
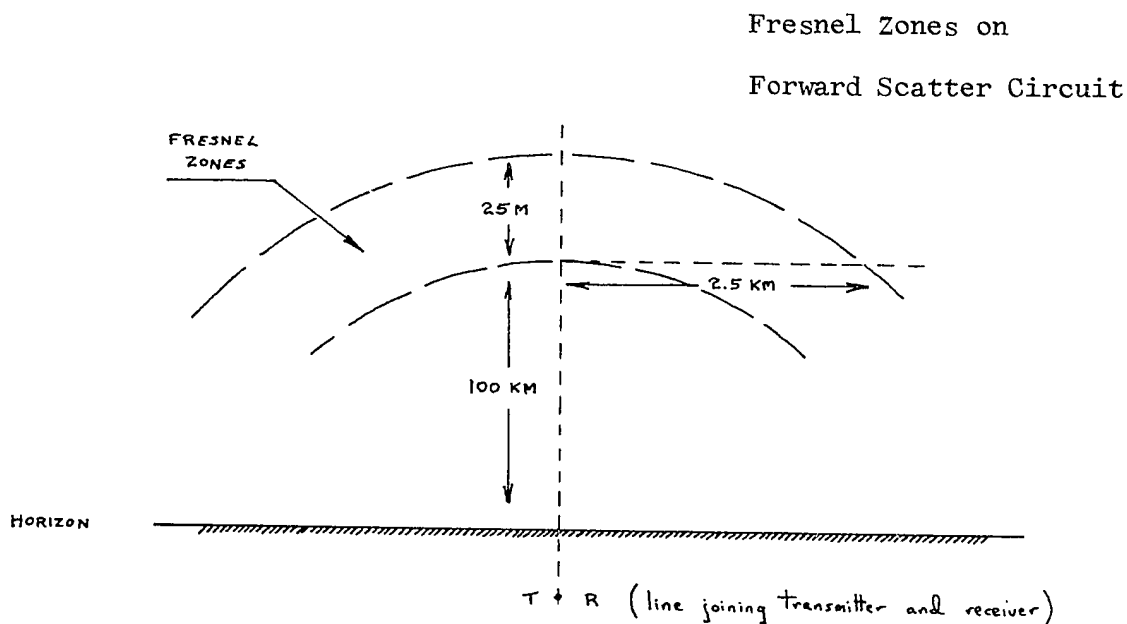
Fig. 6.1

This figure shows a vertical section through the midpoint of a forward scatter path. The transmitter – receiver line is below the surface of the earth because of the curvature of the earth's surface. Calculations show that, for a path length of 1200 Km, each vertical thickness increment of the scattering region of 25 metres introduces an extra phase shift of 2π radians at 40 MHz. In the horizontal plane, each 2.5 Km increment in transverse dimensions introduces a similar relative phase shift. As an example, a scattering region with horizontal dimensions of the order of 250 Km and a thickness of 2.5 Km will produce structure on the ground with a scale size, in both longitudinal and transverse directions, approximately 1/600 that of the scatterers themselves. Larger scattering regions will produce correspondingly smaller structure on the ground, which again may be wavelength limited.

In practice, the scattering region is never unlimited in extent, as has been assumed so far. As a limiting case, consider the situation where the receiving site is in the Fraunhofer diffraction field of the scattering region. The requirement, as it applies to the observations considered here, is that the scattering region subtends a small angle as seen from the receiving site. For this preliminary discussion, the detailed nature of the scattering region is not of importance, except to note that in the case of Fresnel diffraction a very small scale size would be observed on the ground.

The detailed amplitude structure on the ground is governed by the phase differences between the various scattered wave components.
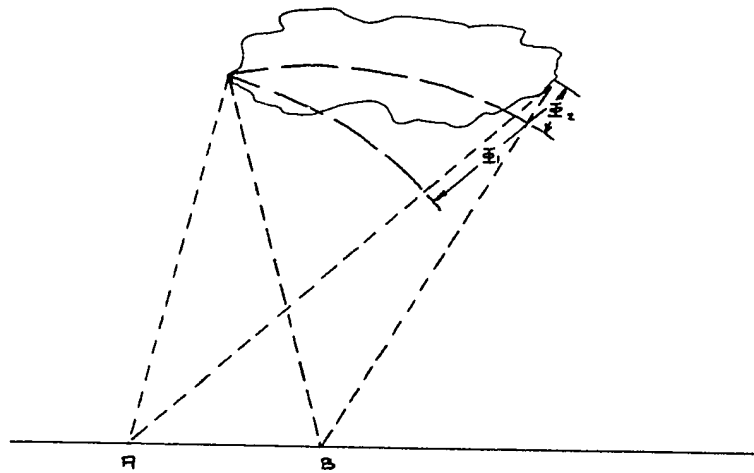
Maximum Phase Path Differences

Fig. 6.2

Referring to Fig. 6.2, the maximum phase differences at points A
and B are Φ_1 and Φ_2 respectively. For a scattering region sufficiently
small, the difference between Φ_1 and Φ_2 may be made arbitrarily small.
If this is the case, it implies that the amplitudes must be
essentially the same at points A and B and so the measured scale
size of the amplitude distribution must be greater than the distance
AB. The finite size of the scattering region may be thought of as
introducing angular coherence into the angular spectrum. The relation-
ship between the size of the scattering region and the minimum scale
size observable on the ground may be found using standard techniques
in diffraction theory. If the spatial number density of individual
scatterers within the scattering region is represented by the
gaussian distribution

$$f(\xi) = \exp\left(-\xi^2/L^2\right) \qquad\qquad 6.2$$

where 2L is the 'width' of the scattering region, then the scale

size of the structure on the ground is given by

$$D = 2z_0\lambda/\pi L \qquad\qquad 6.3$$

where z_0 is the distance from the scattering region to the point

of observation. The diffraction pattern on the ground cannot have

structure smaller than this value, regardless of the nature of the

individual scatterers.

We now investigate the effect of having more than one scattering

region in existence at the same time. Consider first the simplest

case of two regions, each consisting of a random array of scatterers

giving rise to a deep, random modulation of the emerging wavefronts.

It may then be assumed that the phase correlation (coherence in

optical terminology) between the two emerging wavefronts is essentially

zero. The situation is similar to a standard problem in optics

(Born and Wolf, 1959), wherein two apertures are illuminated with

light which has varying degrees of coherence between the two apertures.

The problem is to determine the nature of the diffraction pattern due

to the superposition of the two sources. The result is shown to be

$$I(1,2) = I(1) + I(2) = 2I(1)I(2)\ \gamma\ (1,2)\ \cos\ (\alpha_{12}) \qquad 6.4$$

where $I(1,2)$ is the intensity (power) distribution due to both

    sources

    $I(1)$, $\left[I(2)\right]$ is the power distribution due to the source $I(1)$,

    $\left[I(2)\right]$ alone

    $\gamma(1,2)$ is the coherence between the two sources

    α_{12} is a relative phase factor

If the coherence between the two sources is zero, the resultant intensity field is simply the sum of the two fields taken individually. This result may be extended to any number of sources. A similar result will be found in Ratcliffe (1956). The distribution of power on the ground may thus be described as the sum of the power distributions due to each scattering region alone. It is easily shown that the autocorrelation function of a sum of functions is equal to the sum of the autocorrelation functions of the individual functions. Thus the spatial autocorrelation function of the resultant power distribution is the sum of the autocorrelation functions due to the power distributions from each scattering region.

6.2 Interpretation of the Results Presented in Chapter V

In the last section we deduced the characteristics of the diffraction pattern on the ground from an analysis of the fading records. Now we can consider their implications about ionospheric structure in the light of the conclusions reached in section 6.1.

It is evident from the results of the last chapter that of the three events analyzed, B and C are by far the most completely described. It is also evident, on the basis of measured fading rates, drift velocities, and scale sizes, that these two events are quite dissimilar in character. Event A appears, on the basis of fading rates and scale sizes, similar to event C. The following discussion is thus restricted, primarily, to an interpretation of events B and C, while noting that event C, at least, does not appear to be unique.

Event B:

This event may be divided into two parts: a quasi-periodic part coinciding with the period of maximum amplitude, and non-periodic parts comprising the rest of the event. The non-periodic parts will be discussed first.

Scale size determinations show that the size of the structure of the diffraction pattern on the ground is seldom much larger than the wavelength used. These scale sizes indicate that the effective scattering region was at all times comparable with, or larger in lateral dimensions than, the entire region 'viewed' by the receiving antenna. This distance is approximately 250 Km. The nature of the crosscorrelation functions is consistent with the idea that only a single effective scattering region is in existence at all times.

The time displacements of the crosscorrelation functions are consistent and are compatible with east to west drift velocities ranging from 400 to 1600 m/sec. There is no evidence of more than one velocity component at any time.

This behaviour is very similar to that predicted for scattering from ion-acoustic wave instabilities. According to this theory, (Farley, 1963), only drifts having a positive component in the direction of the electron flow in the auroral electrojet are possible. This flow is generally from east to west under quiet conditions, in agreement with the directions found for the drifts exhibited by this event. The predicted phase velocity of the ion-acoustic waves is close to the velocity of sound in the E region:

360 m/sec. It is the group velocity of these waves which is significant in drift measurements. The relationship between the phase and group velocities is governed by the dispersion relation of the wave process. Farley (1963) has plotted phase velocity as a function of frequency. This enables the group velocity at any frequency to be found from the relation

$$v_g = v_p - \lambda \frac{d}{d\lambda}(v_p) \qquad\qquad 6.5$$

The predicted group velocity at 40 MHz is 420 m/sec. Because of geometrical effects, this gives rise to a diffraction pattern velocity of 840 m/sec. This velocity has been plotted in Fig. 5.7, and is seen to be in good agreement with the experimentally determined range of possible values.

If the scattering does result from ion-acoustic wave instabilities the depth of the scattering region is limited by either the extent of the enhanced electrojet current or by the circuit geometry. In either case, the scattering region is likely to be quite extensive, leading to an approximate volume scattering coefficient of 10^{-9} m^2/m^3. This assumes a depth and vertical thickness of the scattering region of 100 Km and 10 Km respectively. This is close to the value computed for scattering from the equatorial electrojet, at 50 MHz, by Bowles (1963).

A four minute segment of this event, coinciding with the period of maximum amplitude, exhibits unexpected periodic behaviour. We consider first the possibility that some cause, other than auroral scattering, is responsible for the phenomenon. Long duration meteor trails, for example, often produce periodic fading of the received

signal as a result of interference between two different parts of
the trail after distortion by windshears. The Great Whale River –
London circuit 'views' much the same volume of sky as does the
Ottawa – London circuit. For this reason it is of interest to see
if anything unusual occurred on this circuit at the same time as
the periodic signal was observed on the Ottawa – London circuit.
It did not turn out to be possible to check for the presence of a
meteor echo because of the occurrence of a strong type A_2 event
concurrent with the event on the Ottawa – London circuit. However,
the probability of occurrence of a meteor echo of at least four
minutes duration can be estimated using statistics gained from
previous occurrences of meteor echoes of this duration. Meteor
trails of this duration are very rare on the Ottawa – London
circuit, occurring about once per month during non-shower periods.
Also, long-duration meteor trails do not cause coherent fading
for more than a small fraction of their total lifetime. No meteor
showers were predicted for the time that event B occurred. This
gives the probability of finding such an echo within any ten minute
period as approximately 10^{-4}.

If the spatial number density of the individual scatterers is
not representable by a gaussian envelope, it might be thought that
periodic structure could be observed in the measured spatial auto-
correlation function. Consider for example, the diffraction pattern
to be expected from an approximately rectangular distribution of
scatterers. The upper bound of 40m placed on the observed spatial
wavelength implies a minimum lateral extent of the region of

approximately 150 Km. Such a distribution produces maxima in the

diffraction pattern whose intensities decrease as $\sin^2 L/L^2$, where L

is the distance along the ground. This behaviour is not consistent

with the almost constant amplitude of the periodic component of the

signal for a period of approximately four minutes.

Periodic structure of the type observed may be produced by the

interference of waves scattered from two separate regions.   The

separation of the sources must be at least 150 Km in order to produce

the observed spatial wavelength of the structure on the ground. In

order for this process to give rise to observable periodic structure,

it is necessary that some degree of coherence exist between the

signals received from each source. (cf. the last term of equation 6.4).

The degree of coherence between the two signals may be computed from

the relative amplitude of the periodic component in the received

signal. Results range from 0.15 if two waves of comparable intensity

are assumed, to unity if two waves with a 3:1 amplitude ratio are

assumed. Coherence between the received signals may be produced

if the angular sizes of the two sources are sufficiently small that

only a limited part of the angular spectra of the sources contribute

to the observed signal or, if the scattering regions are large, a

considerable degree of coherence exists between the waves scattered

from different parts of the same source. It would seem unlikely

that the former case holds in view of the characteristics derived

for both earlier and later parts of this event. In the latter case

it is surprising that such a high degree of coherence should exist

between wave components scattered from different parts of an extended

scattering region.

Event C:

It has been shown that measured spatial autocorrelation functions may be looked upon as the sum of the individual functions due to each scattering region contributing to the observed signal. The anomalous functions shown in Fig. 5.6 are most easily explained on the basis that at least two separate scattering regions are simultaneously in existence, at least one of which produces a diffraction pattern with a scale size near to that of the transmitted wavelength, and at least one of which produces a diffraction pattern with a scale size of the order of 100 metres. It is inferred, from Eqn. 6.3, that the smaller scale sizes may be identified with scattering regions whose lateral dimensions are comparable with, or larger than, the entire region 'viewed' by the receiving antenna: a distance of several hundred kilometres. The larger scale sizes, on the other hand, may be identified with regions whose lateral dimensions are of the order of 30 Km or less. Such regions subtend angles of less than 3 degrees as seen from the receiving site. It is not possible to tell from the records whether or not the various scattering regions are separated or superimposed in space.

On the basis of the argument presented in Appendix B both easterly and westerly directed drift motions are indicated at all times by the time displacement – antenna separation plots of Figs. 4.17, 4.18, and 4.19. Typical diffraction pattern drift velocities are in the range 0.5 to 10 Km/sec, indicating that the scattering regions

themselves have a range of drift velocities from 0.25 to 5 Km/sec. If these velocities are also typical of event A, it offers an explanation of why no time shifts were observed when a time resolution of 10 msec was used.

In the light of these velocity measurements, spatial autocorrelation functions which appear to have simple gaussian envelopes, such as those shown in Fig. 5.5, must consist of two or more functions which have similar scale sizes.

The nature of the time displacement — antenna separation plots change at least three times during the course of the event, indicating that the direction of drift and number of scattering regions changes at least three times. Fig. 4.14 indicates that the nature of the zero-lag correlation coefficients, and hence minimum scale size, change at least three times during the course of the event. The changes in scale size occur at the same time as the changes in the velocity distribution of the diffraction patterns. Both drift velocity and scale size measurements are thus in agreement with the hypothesis that two or more scattering regions usually contribute to the observed signal amplitude.

It is now possible to draw certain conclusions concerning the nature of the scattering mechanisms responsible for the above event.

The bounds derived for the drift velocities are too high to be compatible with the idea of scattering from random irregularities in electron density which drift with the ambient neutral particle wind velocity in the E region. A large number of E region wind velocity measurements have been made, using both long duration

meteor trails and artificial vapour trails (see, for example, Hines et al., 1965). An upper bound to wind velocities in the region 85 to 120 Km., the region of maximum auroral ionization, appears to be about 150 m/sec. This is lower than the lowest experimental bound of 250 m/sec.

On the other hand, the range of drift directions would appear to be in contradiction with the predictions of the ion-acoustic wave theory (Farley, 1963). As mentioned in connection with event B, only drifts having a positive component in the direction of the electron flow in the auroral electrojet are possible. This flow is generally from east to west under quiet conditions. This event is an example of a weak disturbance, and it is not likely that the electrojet current was sufficiently disturbed to account for velocity components in the west to east direction.

Although it is not possible to find any evidence in the observations presented here for a one to one correspondence between the radio observations and visual observations presented by other workers, it is of interest to note that there is some evidence (Booker et al., 1955; Paulson and Shepherd, 1966) that visual auroral rays consist of a number of 'raylets' which generally are in horizontal motion. The observed horizontal velocities of the raylets range from 0.5 to 24 Km/sec (Paulson and Shepherd, 1966). High sensitivity television studies of auroral arcs (Davis and Hicks, 1964) have also shown that these structures often consist of a large number of short ray-like structures. These structures usually have horizontal motions, occasionally exceeding 50 Km/sec. It

would thus appear that the observations of event C presented here are the result of scattering from structures more akin to the 'raylets' mentioned above than to either ion-acoustic wave structure or to simple 'blobs' of enhanced electron density which move at the surrounding neutral wind velocity.

CHAPTER VII

SUMMARY AND CONCLUSIONS

In this work it has been shown that, in all types of radar and scatter studies, considerable care must be taken in the analysis of the records in order to distinguish between effects due to the individual scatterers and effects due to the geometry of the scattering region as a whole. Specifically, the scale size of the amplitude distribution on the ground has been shown to be determined by the overall extent of the scattering region, regardless of the nature of the individual scatterers. If two or more scattering regions are simultaneously in existence, the scattered fields usually add, and apparently anomalous spatial autocorrelation functions of the scattered fields may result. Drift velocity measurements are representative of the drift velocities of the individual scatterers themselves, but are complicated by the existence of more than one scattering region.

The conclusions reached about the nature of the diffraction patterns from scattering regions in general have been applied to three events observed on the Ottawa – London oblique scatter circuit. Two of these events appear to have similar characteristics while the third differs radically from the other two.

One type of event, which is characterized by slow fading, typically about 15 Hz, has characteristics which are compatible with the hypothesis of scattering by ion-acoustic wave instabilities. This type of instability has previously been shown to be the likely cause of scattering by the equatorial electrojet (Farley, 1963) and some evidence has been produced (Leadabrand, 1965) indicating that this process may be responsible for some types of auroral radar echoes. Drift velocities and volume scattering coefficients deduced in this experiment are in close agreement with the values obtained from studies of the equatorial electrojet.

A four minute period of this event, coinciding with the period of maximum amplitude, exhibited a spatially periodic component in the received signal. It is not possible to give a conclusive explanation of this behaviour, although interference between waves scattered from two widely separated scattering regions appears to be the only likely possibility. A high degree of coherence is required between waves scattered from regions separated by as much as 150 Km.

The other type of event is characterized by rapid fading and occasional very large scale sizes of the structure on the ground. The large scale sizes imply the existence of scattering regions whose horizontal dimensions are sometimes less than 30 Km. A range of diffraction pattern drift velocities have been observed. Typical drift velocities range from 0.5 to 10 Km/sec. These observations are incompatible with either scattering from ion-acoustic wave instabilities or from 'blobs' of enhanced electron density drifting with the surrounding wind velocity. A similarity has been noted

between these drift velocities and those reported for the fine structure of visual auroral forms.

These results have been based on relatively few observations. A longer sequence of observations is needed in order to show if the observed events are indeed restricted to only two types. It would be of interest to carry out further observations using antennas with considerably larger spatial separations in order to set more accurate limits on the larger scale sizes observed. The possibility of critical reflection, in events similar to event C, arises if the dimensions of the scattering regions are shown to be sufficiently small. Further information can be obtained through simultaneous measurements. similar to those made by Lyon (1967), at different scattering angles and through doppler measurements of the received signals. It would be of considerable interest to carry out high resolution measurements, similar to those described in this thesis, simultaneously with the above types of observations.

In conclusion, obliquely scattered auroral echoes have been shown to consist of at least two separate types. One type of event appears due to scattering by ion-acoustic wave instabilities, while the other appears due to scattering by irregularities with large drift velocities and occasional small dimensions of the overall scattering regions. No evidence has been found, in the limited number of events studied, for scattering from simple 'blobs' of enhanced ionization which drift with the local wind velocity.

APPENDIX A

BOUNDS ON POSSIBLE DRIFT VELOCITIES

The following terms have been previously defined in Chapter 5. They are given again here for convenience.

V   Actual velocity of the diffraction pattern over the ground.

V'   Apparent velocity of the diffraction pattern between two spaced antennas, as measured from crosscorrelation function time displacements.

V'_c Velocity an unchanging diffraction pattern would need in order to give the observed fading rate. $V'_c = \xi_0/\tau_0$ where ξ_0 and τ_0 satisfy the relation $\rho(\xi,o) = \rho(o,\tau)$ A.1

V_c V'_c as seen by an observer moving at the velocity V. This is a measure of the rate of change of the diffraction pattern with time.

Subscripts t and l will refer to the transverse and longitudinal components of the above variables, with respect to the expected direction of arrival of the scatter signals. This direction is at right angles to the line joining the antennas.

The simplest case is where the pattern is assumed to change with time but where the scale size is independent of direction over the ground. This is called an isometric pattern. In this case

$$\frac{1}{(V')^2} = \frac{1}{(V'_l)^2} + \frac{1}{(V'_t)^2}$$

78

It is easily shown from this that $V' \leq V'_t$

But $V = (V'_c)^2_t / V'$ so that $V \geq (V'_c)^2_t / V_t$ A.2

Now $VV' = V^2_c + V^2$

and in this case $V_c \geq 0$

so that $V' \geq V$

But $V'_t \geq V'$

so that $V'_t \geq V'$ A.3

From Eqn. A.2 and A, 3 we finally have

$$\frac{(V'_c)^2_t}{V'_t} \leq V \leq V'_t \qquad \text{A.4}$$

Because of the geometry of the Ottawa - London circuit, the diffraction pattern on the ground must be highly anisotropic. The axial ratio of the correlation ellipse is approximately six, with the minor axis in the direction of the line joining the antenaas. In the notation of Phillips and Spencer, $r \sim 6$ and $\psi \sim 0$ degrees.

For this anisotropic case, the 'true' drift velocity is given

$$V = \frac{[1 + (r^2 - 1)\cos^2\psi][\cos(\Phi - \Phi_a)](V'_c)^2_t}{[1 + (r^2 - 1)\cos^2(\Phi - \psi)]V'_a}$$

where Φ is the true direction of drift, and

       Φ_a is the apparent direction of drift.

Since $r^2 \gg 1$, $\psi \sim 0$, and $V_a' = V_t' \cos\Phi_a$, we may write this as

$$V \sim \left(\frac{(V_c')^2_t}{V_t'} \right) \left(\frac{r^2 \cos(\Phi - \Phi_a)}{1 + r^2\cos^2\Phi} \right) \left(\frac{1}{\cos\Phi_a} \right)$$

In our case we may write

$$\tan\Phi \sim r^2 \tan\Phi_a \qquad \text{since} \quad \psi \sim 0$$

so that

$$\Phi \gg \Phi_a \qquad \text{since} \quad r^2 \gg 1$$

Thus

$$\cos(\Phi - \Phi_a) \leq \cos\Phi \qquad \text{if} \quad \Phi \leq 60^\circ$$

and finally

$$V \geq \frac{(V_c')^2_t}{V_t'} \left(\frac{r^2 \cos^2\Phi}{(1 + r^2\cos^2\Phi)(\cos\Phi_a)} \right)$$

The term $\dfrac{r^2 \cos^2\Phi}{(1 + r^2 \cos^2\Phi)(\cos\Phi_a)}$ has a magnitude always greater than

approximately 1 for all directions of drift Φ, except for a region within 1 degree of 90 degrees. Thus, as for the isometric case, we may write

$$V \geq \frac{(V_c')^2_t}{V_t'} \qquad\qquad\qquad \text{A.5}$$

A derivation, similar to that leading to Eqn. A.3, gives again

$$V_t' \geq V$$

so that in this case also, we have

$$\frac{(V_c')^2_t}{V_t'} \leq V \leq V_t' \qquad\qquad\qquad \text{A.6}$$

Bounds may also be placed on the fading velocity V_c.

We may write $\quad V_c^2 = VV' - V^2$

If $\quad V = V_t'$

then $V_c^2 = V_t'V' - (V_t')^2$

But $\qquad V' \leq V_t' \qquad\qquad$ so that $\qquad\qquad V_c^2 \leq (V_t')^2 - (V_t')^2$

$$= 0$$

and finally $\qquad V_c = 0 \qquad\qquad\qquad\qquad\qquad\qquad\qquad\qquad$ A.7

If, on the other hand $\qquad V = \dfrac{(V_c')_t^2}{V_t'}$

then
$$V_c^2 = \frac{(V_c')_t^2}{V_t'} \cdot V' - \left(\frac{(V_c')_t^2}{V_t'}\right)^2$$

$$\leq \frac{(V_c')_t^2}{V_t'} \cdot V_t' - \left(\frac{(V_c')_t^2}{V_t'}\right)^2$$

$$\leq (V_c')_t^2 \left[1 - \left(\frac{(V_c')_t}{V_t'}\right)^2\right] \qquad\qquad\qquad \text{A.8}$$
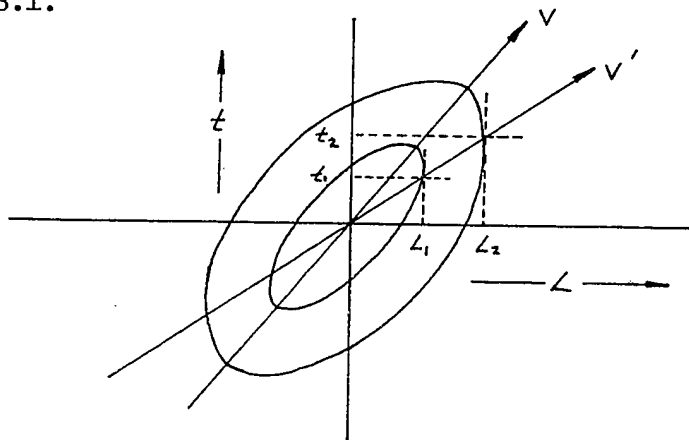
From Eqn. A.7 and A.8 we may finally write

$$0 \leq V_c \leq (V_c')_t \left[1 - \left(\frac{(V_c')_t}{V_t'}\right)^2\right]^{\frac{1}{2}} \qquad\qquad \text{A.9}$$

APPENDIX B

TIME DISPLACEMENTS RESULTING FROM MORE THAN ONE SCATTERING REGION

The relationship between antenna separation L and the corresponding crosscorrelation function time displacement t is shown in the L-t diagram of Briggs and Phillips (1950). This is illustrated in Fig. B.1.
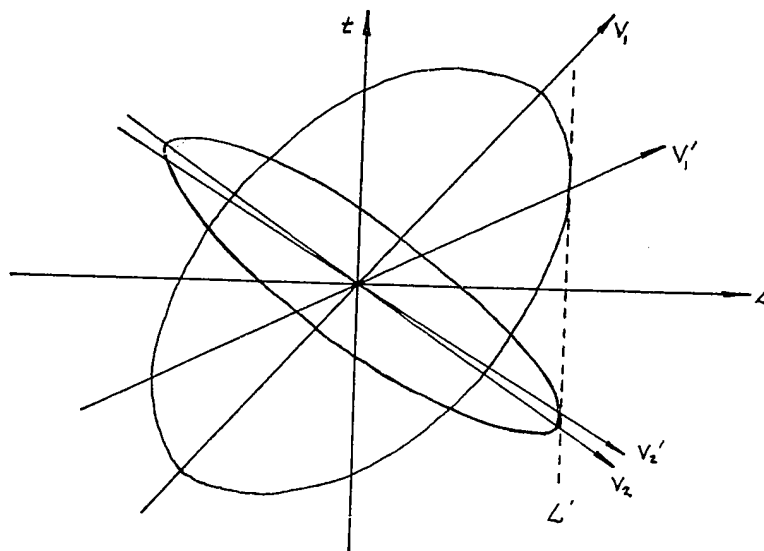

The L-t diagram

Fig. B.1

Observed time displacements correspond to the times at which vertical lines (representing the time axis of the temporal crosscorrelation functions) at various antenna separations intersect the V' line. It has been shown in Chapter 6 that two scattering regions will usually give rise to a diffraction pattern on the ground which is the sum of the patterns due to each region separately. In this

82

case, the following L-t diagram may be drawn:

The L-t diagram for Two Superimposed Patterns.

Fig. B.2

The resultant crosscorrelation functions at any antenna separation L may be found by summing the amplitudes of the two characteristic ellipses along a vertical line drawn through L. A variety of results may be obtained depending upon the orientation of the characteristic ellipses (proportional to pattern drift velocity) and the eccentricity of the ellipses (proportional to the time rate of change of the pattern). By way of illustration we assume that the resultant diffraction pattern on the ground is the sum of two diffraction patterns with the following characteristics:

A. Amplitude: 2 units

   Scale size: 15 metres

   Temporal autocorrelation function width: 10 msec

   Drift velocity: 10^4 m/sec to the left

B. Amplitude: 1 unit

    . Scale size: 45 metres

    Temporal autocorrelation function width: 32 msec

    Drift velocity: 10^4 m/sec to the right

The resultant correlation functions for antenna separations of o

(autocorrelation), 2, 4, and 6 wavelengths are shown in Fig. B.3, and

the resultant displacements of the peaks in the correlation functions,

as a function of antenna separation, are shown in Fig. B.4.

It is seen that Fig. B.4 is a good approximation to Fig. 4.17.

It is possible to explain the more complex plots of Figs. 4.18 and

4.19 on the assumption that three or more distinct scattering regions

were simultaneously in existence. Generally, patterns with drift

components in opposite directions are required to produce plots similar

to Fig. 4.17, in which both positive and negative time shifts are ob-

served.

The slopes of the above plots, in regions not near the turning

points of the curves, give approximations to the velocities of the

separate scattering regions. A one-to-one correspondence between this

type of velocity measurement and specific scattering regions breaks

down if the number of scattering regions is large, but the derived

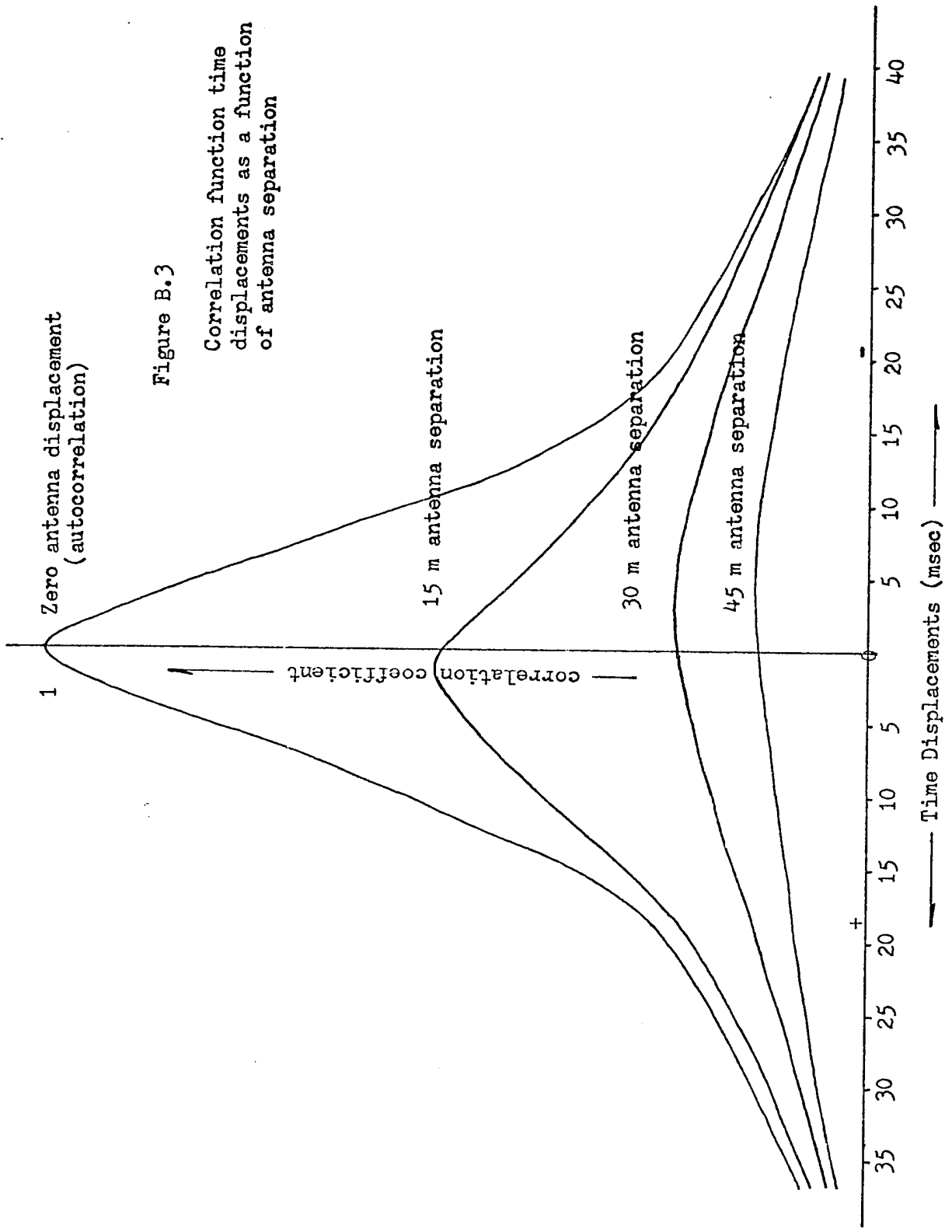velocities may be looked upon as typical of the regions as a whole.

Figure B.3

Correlation function time displacements as a function of antenna separation
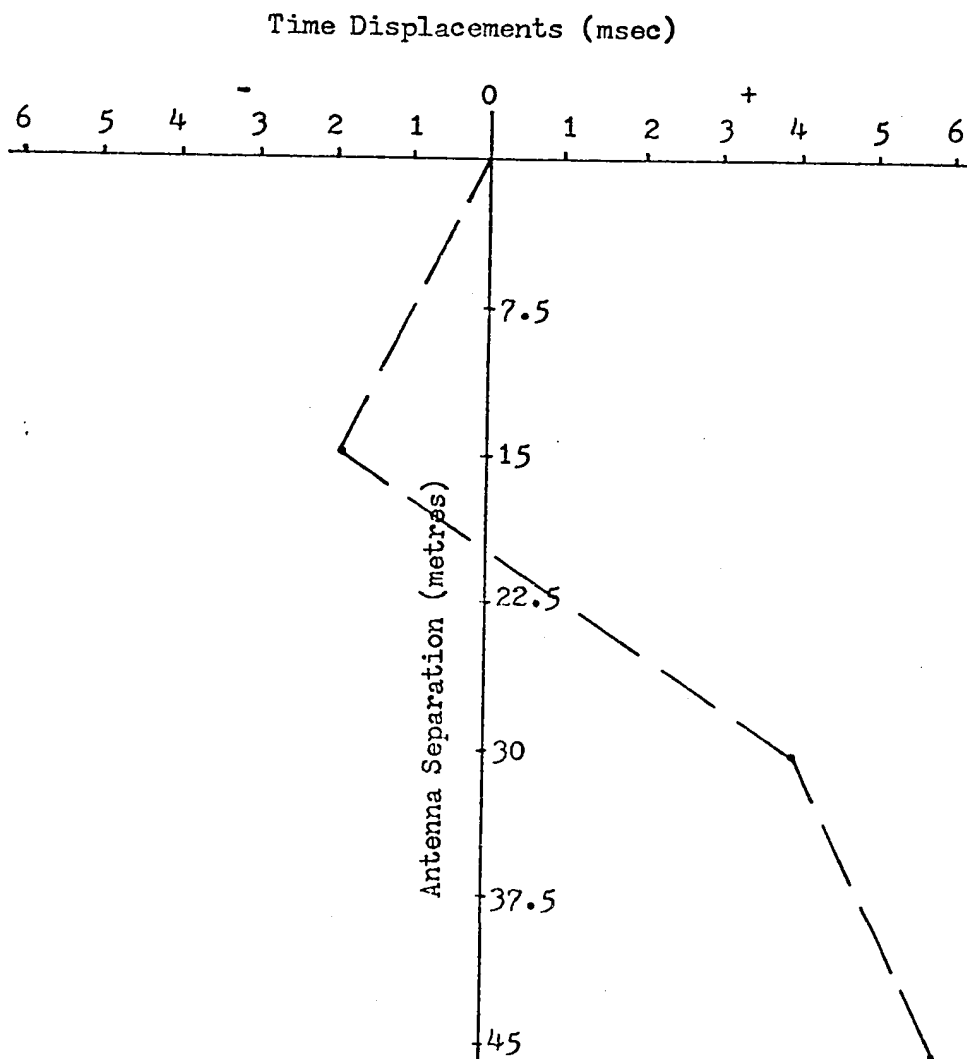
Figure B.4

Time Displacements, as a Function of Antenna

Separation, of Peaks in Correlation Functions